

MARTIN MARIETTA ENERGY SYSTEMS LIBRARIES



3 4456 0355012 8

ORNL/TM-11691

# oml

**OAK RIDGE  
NATIONAL  
LABORATORY**

**MARTIN MARIETTA**

## Corrosion Behavior of Continuous-Filament-Wound Ceramic Composite Tubes

J. I. Federer

OAK RIDGE NATIONAL LABORATORY  
 CENTRAL RESEARCH LIBRARY  
 CIRCULATION SECTION  
 4500N ROOM 173

**LIBRARY LOAN COPY**  
 DO NOT TRANSFER TO ANOTHER PERSON  
 If you wish someone else to see this  
 report, send in name with report and  
 the library will arrange a loan.

MANAGED BY  
MARTIN MARIETTA ENERGY SYSTEMS, INC.  
FOR THE UNITED STATES  
DEPARTMENT OF ENERGY

This report has been reproduced directly from the best available copy.

Available to DOE and DOE contractors from the Office of Scientific and Technical Information, P.O. Box 62, Oak Ridge, TN 37831; prices available from (615) 576-8401, FTS 626-8401.

Available to the public from the National Technical Information Service, U.S. Department of Commerce, 5285 Port Royal Rd., Springfield, VA 22161.

This report was prepared as an account of work sponsored by an agency of the United States Government. Neither the United States Government nor any agency thereof, nor any of their employees, makes any warranty, express or implied, or assumes any legal liability or responsibility for the accuracy, completeness, or usefulness of any information, apparatus, product, or process disclosed, or represents that its use would not infringe privately owned rights. Reference herein to any specific commercial product, process, or service by trade name, trademark, manufacturer, or otherwise, does not necessarily constitute or imply its endorsement, recommendation, or favoring by the United States Government or any agency thereof. The views and opinions of authors expressed herein do not necessarily state or reflect those of the United States Government or any agency thereof.

Metals and Ceramics Division

CORROSION BEHAVIOR OF CONTINUOUS-FILAMENT-WOUND  
CERAMIC COMPOSITE TUBES

J. I. Federer

Date Published: May 1991

NOTICE: This document contains information of a preliminary nature.  
It is subject to revision or correction and therefore does not  
represent a final report.

Prepared for the  
Assistant Secretary for Conservation and Renewable Energy  
Office of Industrial Technologies  
ED 01 12 00 0

Prepared by the  
OAK RIDGE NATIONAL LABORATORY  
Oak Ridge, Tennessee 37831-6285  
managed by  
MARTIN MARIETTA ENERGY SYSTEMS, INC.  
for the  
U.S. DEPARTMENT OF ENERGY  
under Contract DE-AC05-84OR21400



3 4456 0355012 8



## CONTENTS

	Page
LIST OF TABLES .....	v
LIST OF FIGURES .....	vii
INTRODUCTION .....	2
MATERIALS .....	3
EQUIPMENT AND PROCEDURES .....	4
RESULTS .....	10
VISUAL APPEARANCE .....	10
DIMENSIONAL CHANGES .....	16
OPTICAL MICROSCOPY .....	22
ELECTRON MICROPROBE ANALYSIS .....	32
X-RAY DIFFRACTION ANALYSIS .....	37
DISCUSSION .....	39
SUMMARY AND CONCLUSIONS .....	41
REFERENCES .....	43



## LIST OF TABLES

Table		Page
1	Ceramic composite specimens . . . . .	4
2	Thermal treatments in air and the corrosive atmosphere . . . . .	11
3	Temperatures (°C) in three positions in the furnace tubes in air and in the corrosive atmosphere . . . . .	15
4	X-ray diffraction results . . . . .	38



## LIST OF FIGURES

Figure		Page
1	Typical as-fabricated hoop- and helical-wound specimens . . . . .	5
2	Arrangement for thermal treatments . . . . .	6
3	Arrangement for controlling flow of corrosion atmosphere constituents . . . . .	7
4	Thermal treatment plan for ceramic composite specimens in either air or air-3.4 wt % H <sub>2</sub> O-0.01 wt % Na <sub>2</sub> CO <sub>3</sub> atmosphere . . . . .	8
5	Hoop-wound specimens after exposure to the corrosive atmosphere for 500 h. B6, Al <sub>2</sub> O <sub>3</sub> matrix; D18, ZrO <sub>2</sub> matrix . . . . .	12
6	Helical-wound specimens with ZrO <sub>2</sub> matrices after exposure to the corrosive atmosphere for 500 h . . . . .	13
7	Helical-wound specimens with ZrO <sub>2</sub> matrices after exposure to the corrosive atmosphere for 300 h. I2, SnO <sub>2</sub> coating; K3, ZrO <sub>2</sub> coating . . . . .	14
8	Dimensional changes in hoop-wound specimens A5 and B6 with Al <sub>2</sub> O <sub>3</sub> matrices . . . . .	17
9	Dimensional changes in hoop-wound specimens C7 and D18 with ZrO <sub>2</sub> matrices . . . . .	18
10	Dimensional changes in hoop-wound (A5) and helical-wound (E9) specimens with Al <sub>2</sub> O <sub>3</sub> matrices tested in air . . . . .	19
11	Dimensional changes in helical-wound specimens G2, F15, and H3 with ZrO <sub>2</sub> matrices . . . . .	20
12	Dimensional changes in helical-wound specimens J2 and K3 with ZrO <sub>2</sub> matrices . . . . .	21
13	Dimensional changes in helical-wound specimen I2 with a ZrO <sub>2</sub> matrix . . . . .	22
14	Specimen A5 after testing in air . . . . .	23
15	Specimen C7 after testing in air . . . . .	24
16	Specimen G2 after testing in air . . . . .	25

Figure	Page
17 Specimen B6 after corrosion testing . . . . .	26
18 Specimen D18 after corrosion testing . . . . .	27
19 Specimen F15 after corrosion testing . . . . .	28
20 Specimen H3 after corrosion testing . . . . .	29
21 Specimen 12 after corrosion testing . . . . .	30
22 Specimen K3 after corrosion testing . . . . .	31
23 Electron microprobe analysis of specimen B6 after corrosion testing . . . . .	33
24 Electron microprobe analysis of specimen F15 after corrosion testing . . . . .	34
25 Electron microprobe analysis of specimen K3 after corrosion testing . . . . .	36

## CORROSION BEHAVIOR OF CONTINUOUS-FILAMENT-WOUND CERAMIC COMPOSITE TUBES\*

J. I. Federer

### ABSTRACT

Ceramic composites are being developed for heat exchanger tubes in industrial furnaces. Because industrial furnace atmospheres often contain alkali compounds, the corrosion behavior of ceramic composites was investigated in an oxidizing atmosphere containing  $\text{Na}_2\text{CO}_3$  vapor. The composites, in the form of tubes, consisted of  $\text{Al}_2\text{O}_3$ -20 wt %  $\text{ZrO}_2$  continuous-filament-wound bodies impregnated with  $\text{Al}_2\text{O}_3$  or  $\text{ZrO}_2$  matrices. The matrices contained 20 to 30% porosity. The tubes were thermally cycled three or four times between 20 and  $1150^\circ\text{C}$  with cumulative holding times, at  $1150^\circ\text{C}$ , of 300 or 500 h. One set of specimens was thermally cycled in air for comparison with a similar set thermally cycled in the  $\text{Na}_2\text{CO}_3$ -containing atmosphere. Specimens heat-treated in air had almost no visual evidence of degradation, but specimens exposed to the corrosive atmosphere exhibited bending, nonuniform expansion, cracking, and spalling. Dimensional changes in specimens heat-treated in air were  $<\pm 0.5\%$  compared to values up to  $+6\%$  in specimens exposed to the corrosive atmosphere. In specimens with  $\text{ZrO}_2$  matrices, Na was found to be concentrated at the interfaces between matrix and filaments, indicating that the matrix porosity allowed access of the atmosphere to the filaments. In the specimen with an  $\text{Al}_2\text{O}_3$  matrix, Na was concentrated on the outer surface, indicating high reactivity between Na and  $\text{Al}_2\text{O}_3$ . X-ray diffraction analysis showed that several sodium aluminates had formed by reaction of  $\text{Na}_2\text{CO}_3$  with the  $\text{Al}_2\text{O}_3$  matrix and high  $\text{Al}_2\text{O}_3$  filaments, but no sodium zirconates were detected. The degradation of the specimens was attributed to the volume increases associated with formation of sodium aluminates. These results indicate that exposure of the ceramic composites to Na-containing industrial furnace atmospheres at temperatures as high as were used in these tests would cause corrosion and dimensional changes.

---

\*Research sponsored by the U.S. Department of Energy, Assistant Secretary for Conservation and Renewable Energy, Office of Industrial Technologies, Industrial Energy Efficiency Division, under contract DE-AC05-84OR21400 with Martin Marietta Energy Systems, Inc.

## INTRODUCTION

An advanced waste heat recuperator is being developed by Babcock & Wilcox Company (B&W) under contract to the U.S. Department of Energy.<sup>1,2</sup> The recuperator is intended to recover heat from the fouling and corrosive flue gases of industrial furnaces. The heat will be recovered in the form of heated air, which will be used for various applications. This preheated air could be used as combustion air for furnace burners, wherein the resulting higher flame temperature reduces fuel consumption. Alternatively, the preheated air could be used to drive a gas turbine. These or other applications require a steady, uninterrupted supply of hot air. The heat exchanger tubes, therefore, are critical components of the recuperator system. The tubes must be dimensionally stable, strong, thermal shock resistant, and corrosion resistant during exposure to high-temperature, thermal cycling, and corrosive flue gases of aluminum remelt furnaces, steel soaking pits, waste incinerators, and similar furnaces.

Selection of materials for the heat exchanger tubes involved exposure tests of various Si-based and oxide ceramics in industrial furnaces. These tests revealed that SiC and Si<sub>3</sub>N<sub>4</sub> ceramics corroded severely in furnace environments containing alkali compounds (e.g., aluminum remelt furnaces), and that the corrosion of oxide ceramics increased with increasing SiO<sub>2</sub> content of the ceramic.<sup>3</sup> Based on these results and other information developed by B&W, Al<sub>2</sub>O<sub>3</sub> and stabilized ZrO<sub>2</sub> were selected as matrix materials in ceramic composites with continuous filaments of PRD166\* (Al<sub>2</sub>O<sub>3</sub>-20 wt % ZrO<sub>2</sub>). Fabrication of composites by a proprietary sol-gel method is being developed by B&W. The fabrication variables include the filament-winding pattern and coatings to seal inherent matrix porosity.

---

\*DuPont Corporation, Wilmington, Del.

In addition to mechanical properties and corrosion testing being performed by B&W during fabrication development, 11 specimens were corrosion tested at ORNL. Previous testing of similar specimens in an oxidizing atmosphere containing  $\text{Na}_2\text{CO}_3$  vapor had revealed considerable dimensional stability in some similar ceramic composite specimens.<sup>3</sup> The purpose of the present tests was to assess the dimensional stability and corrosion resistance of possibly improved specimens at temperatures of interest to the heat exchanger program. Unlike the previous work, testing involved thermal treatments in both air and a potentially corrosive atmosphere in an attempt to separate thermal and corrosion effects. Dimensional stability was the principal measured response. Various techniques such as optical microscopy, X-ray diffraction, and microchemical analysis were used to develop an understanding of observed changes in dimensions.

## MATERIALS

Eleven tubular ceramic composite specimens were tested. Each specimen had PRD166 continuous filaments in an  $\text{Al}_2\text{O}_3$  or  $\text{ZrO}_2$  (stabilized with  $\text{Y}_2\text{O}_3$ ) matrix (Table 1). The  $\text{ZrO}_2$  was only partially stabilized, as shown later in this report. The specimens were prepared by first hoop or helical wrapping the continuous filament on a mandrel. Hoop winding used an  $\sim 0^\circ$  angle of advance (screw angle); whereas, helical winding used an  $\sim 30^\circ$  angle of advance. Interlocking fiber wraps were achieved by helical wrapping in both directions along the axis of the mandrel. The filament was impregnated with the matrix material by a proprietary sol-gel process, then sintered. Sintering was performed at a low temperature to minimize reaction between the matrix and the filaments. As a result, the matrices contained 20 to 30% porosity. Typical as-fabricated hoop- and helical-wound specimens are shown in Fig. 1.

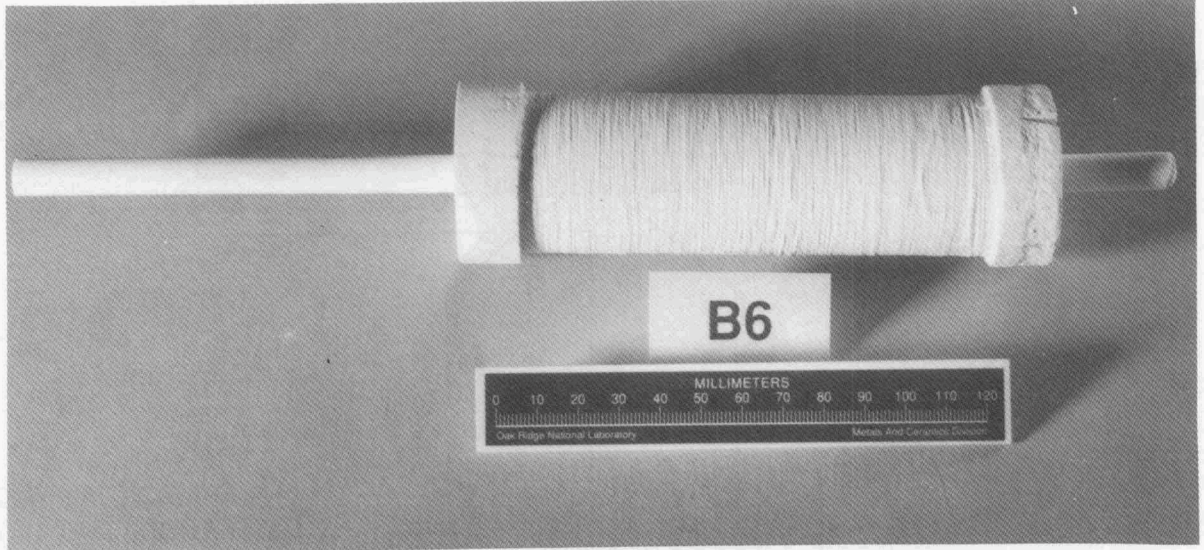
Table 1. Ceramic composite specimens

Specimen number	Matrix material	Filament winding pattern	Coating
A5	Al <sub>2</sub> O <sub>3</sub>	Hoop	None
B6	Al <sub>2</sub> O <sub>3</sub>	Hoop	None
C7	ZrO <sub>2</sub>	Hoop	None
D18	ZrO <sub>2</sub>	Hoop	None
E9	Al <sub>2</sub> O <sub>3</sub>	Helical	None
F15	ZrO <sub>2</sub>	Helical	None
G2	ZrO <sub>2</sub>	Helical	None
H3	ZrO <sub>2</sub>	Helical	None
I2	ZrO <sub>2</sub>	Helical	SnO <sub>2</sub>
J2	ZrO <sub>2</sub>	Helical	ZrO <sub>2</sub>
K3	ZrO <sub>2</sub>	Helical	ZrO <sub>2</sub>

### EQUIPMENT AND PROCEDURES

Thermal treatments were performed in two similar furnaces, each having three alumina tubes for specimen containment. A furnace with temperature control and monitoring equipment is shown schematically in Fig. 2. An auxiliary calibrated type S thermocouple was temporarily installed in each tube when the furnace was at equilibrium to measure the temperature of the gas adjacent to the specimens. Components used to control and measure constituents of the corrosive atmosphere are shown schematically in Fig. 3. Air was metered with conventional tube and float flowmeters. A solution of H<sub>2</sub>O–0.5 wt % Na<sub>2</sub>CO<sub>3</sub>, metered by a tubing pump, dripped into platinum cups at about 1000°C, where vaporization occurred. The nominal composition of the corrosive atmosphere was N<sub>2</sub>–22.5 wt % O<sub>2</sub>–3.4 wt % H<sub>2</sub>O–0.01 wt % Na<sub>2</sub>CO<sub>3</sub>. This atmosphere

YP9402



YP9401

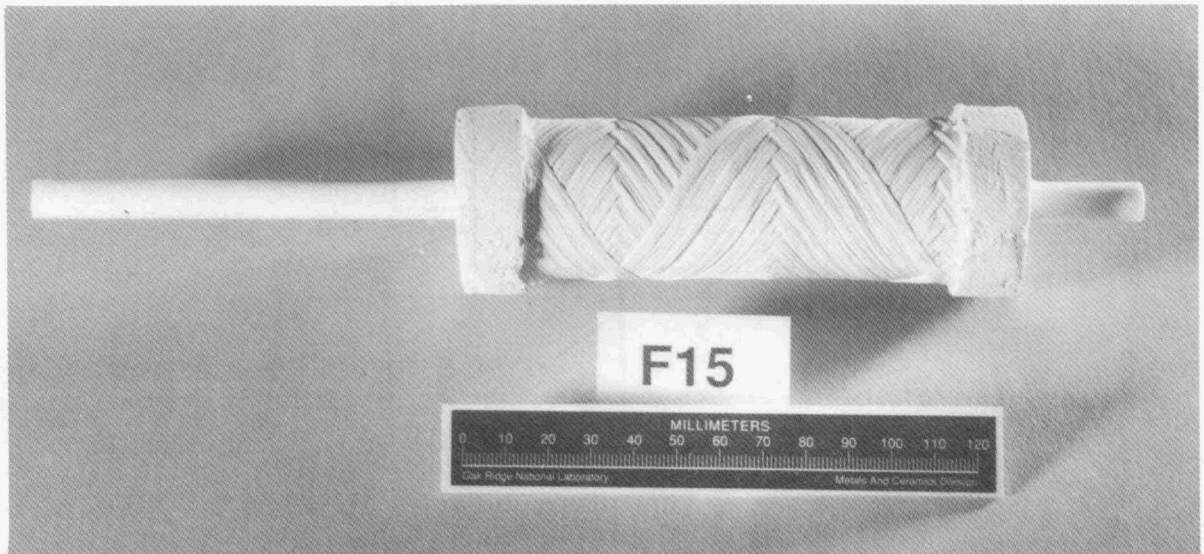


Fig. 1. Typical as-fabricated hoop- and helical-wound specimens.

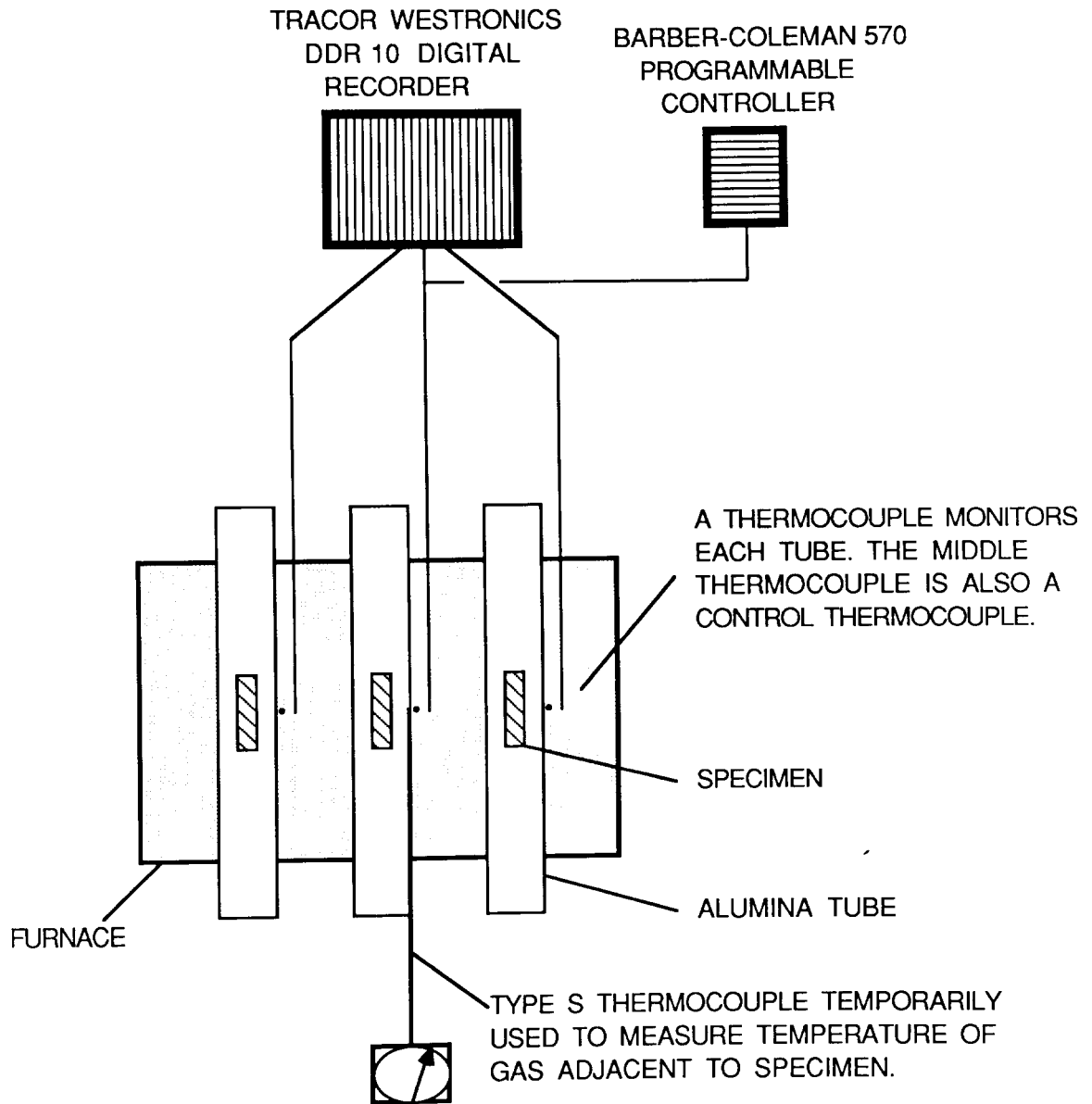


Fig. 2. Arrangement for thermal treatments.

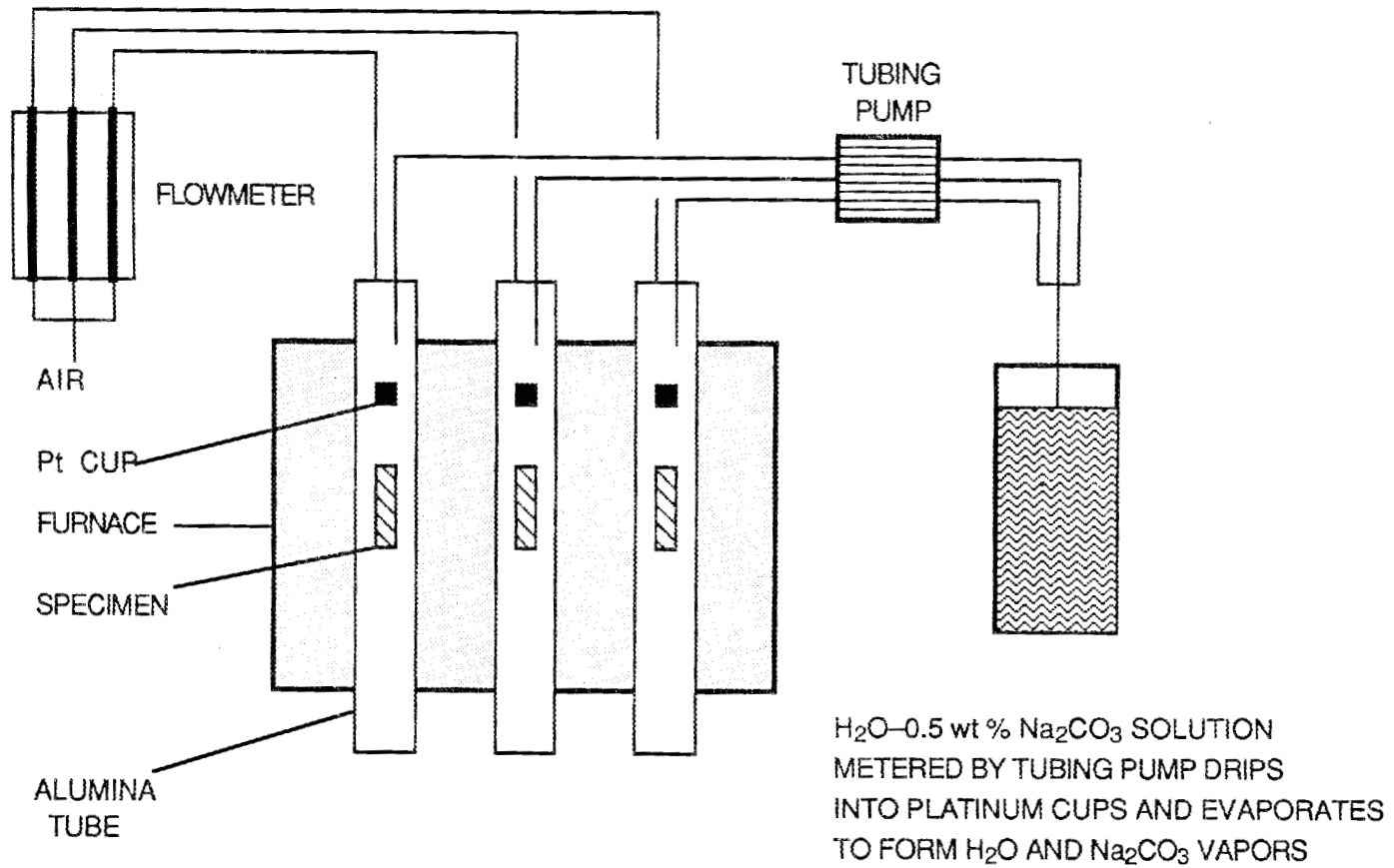


Fig. 3. Arrangement for controlling flow of corrosion atmosphere constituents.

was chosen because alkali oxides are expected to be present in an oxidizing atmosphere in many of the applications where the ceramic composites would be used; for example, municipal waste incinerators.

Specimens were subjected to the thermal treatments shown in Fig. 4. Each thermal cycle involved a programmed maximum heating rate of about  $47^{\circ}\text{C}/\text{h}$  to a nominal maximum temperature of 1150 to  $1160^{\circ}\text{C}$ , a specific holding time at the maximum temperature, and natural furnace cooling. The maximum temperatures of the two outer specimens in each furnace were 10 to  $25^{\circ}\text{C}$  lower than that of the center specimen.

Tubular specimens had nominal dimensions of 41 mm OD  $\times$  120 mm long with wall thicknesses varying from about 3 to 10 mm. The ends were closed by cemented ceramic plugs. Diameters were measured with an optical comparator at eight approximately

ORNL-DWG 90-17133

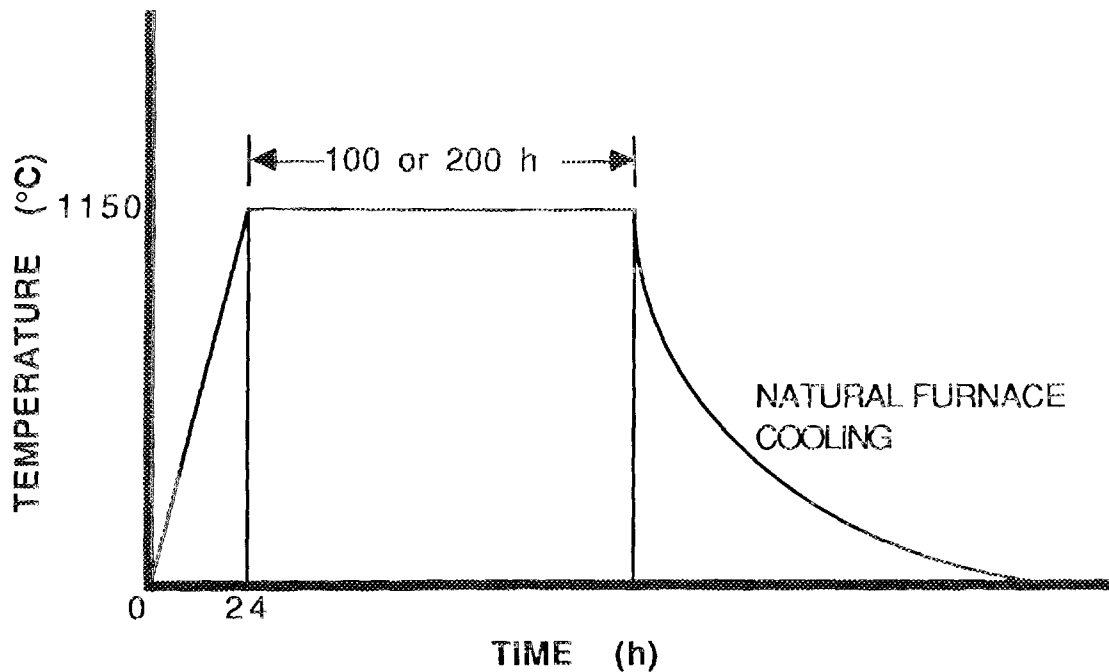


Fig. 4. Thermal treatment plan for ceramic composite specimens in either air or air-3.4 wt %  $\text{H}_2\text{O}$ -0.01 wt %  $\text{Na}_2\text{CO}_3$  atmosphere.

equally spaced circumferential positions at the longitudinal center and at positions  $25 \pm 2$  mm on each side of center. The length of the specimens, including the end plugs, was measured at four circumferential positions with micrometers. Dimensions were measured before and after each thermal treatment described in Fig. 4.

Similar specimens were used for exposure to air and the corrosive atmosphere, so that the effects (if any) of each atmosphere could be determined. A set of specimens was exposed to air, metered at  $6000 \text{ cm}^3/\text{min}$  into each furnace tube. Metering conditions were about  $21^\circ\text{C}$  and 1 atm. The flowmeters were calibrated with a secondary standard, which had been calibrated with a volume chamber at  $21^\circ\text{C}$  and 1 atm. Another set was exposed to a mixture of air,  $\text{H}_2\text{O}$ , and  $\text{Na}_2\text{CO}_3$  vapor. Water and  $\text{Na}_2\text{CO}_3$  were metered as a solution as described above. The solution was prepared with water having an electrical resistance of  $0.5 \text{ M}\Omega$  or more (equivalent to water containing 0.9 ppm NaCl or less) by passing the water through a mixed resin column (Barnstead D0809\*). The composition of the solution was prepared with an accuracy of  $0.5 \pm 0.01 \text{ wt } \% \text{ Na}_2\text{CO}_3$  in  $4000\text{-cm}^3$  batches by measuring both the water and the  $\text{Na}_2\text{CO}_3$  with an accuracy of 0.25% or better.

The solution was metered by a tubing pump. A pump for each furnace delivered approximately  $0.25 \text{ cm}^3/\text{min}$  of solution to each of three furnace tubes. Because the resistance of the lines from the pump to the drip tubes varied slightly, the actual drip rate was not the same in each furnace tube. Measurements of drip rates in special 6- to 8-h experiments before and after each thermal treatment showed that the values were within  $0.25 \pm 0.02 \text{ cm}^3/\text{min}$ . The total volume of solution consumed was determined by refilling the solution container to a reference mark as required.

---

\*Barnstead Company, subsidiary of Sybron Corporation, Newton, Mass.

## RESULTS

### VISUAL APPEARANCE

A set of five specimens was tested in air at about 1150°C for 500 h. As shown in Table 2, these specimens were heated sequentially for 100, 200, and 200 h, a total of 500 h including three thermal cycles between 20°C and the maximum temperature. A set of six specimens was tested in the corrosive atmosphere, four for 500 h with four thermal cycles and two for 300 h with three thermal cycles. Specimens exposed to air alone exhibited no visual evidence of degradation, such as bending, cracking, or spalling; however, each type of degradation occurred in specimens exposed to the corrosive atmosphere, as shown in Figs. 5–7. Figure 5 shows slight bending with no cracks in B6, and slight bending, cracking, and spalling in D18. Figure 6 shows cracking and spalling of outer layers of F15, and cracking and severe bending of H3. Figure 7 shows numerous cracks and spalling of I2, and bending and severe cracking of K3. The cracks in all specimens were perpendicular to the filaments.

Because specimens exposed to air alone exhibited none of these modes of degradation, and because the damage in four specimens was mostly above the midpoint, the possibility that the method of introducing the H<sub>2</sub>O–0.5 wt % Na<sub>2</sub>CO<sub>3</sub> solution caused unusual temperature gradients was investigated. Figure 3 shows that the solution dripped into platinum cups to be vaporized. The cups were located ~50 mm (2 in.) above the tops of the specimens, so there was concern that the steam caused significant temperature transients. This possibility was investigated by measuring temperatures circumferentially and axially in the vicinity of a specimen with either air or the corrosive atmosphere flowing. An auxiliary thermocouple was used, as shown in Fig. 2, to measure the temperatures. Table 3 shows that the corrosive atmosphere caused no substantial difference in temperature compared to air alone. The largest temperature difference at any location was only 4°C. Table 3 also illustrates the axial temperature gradient imposed on

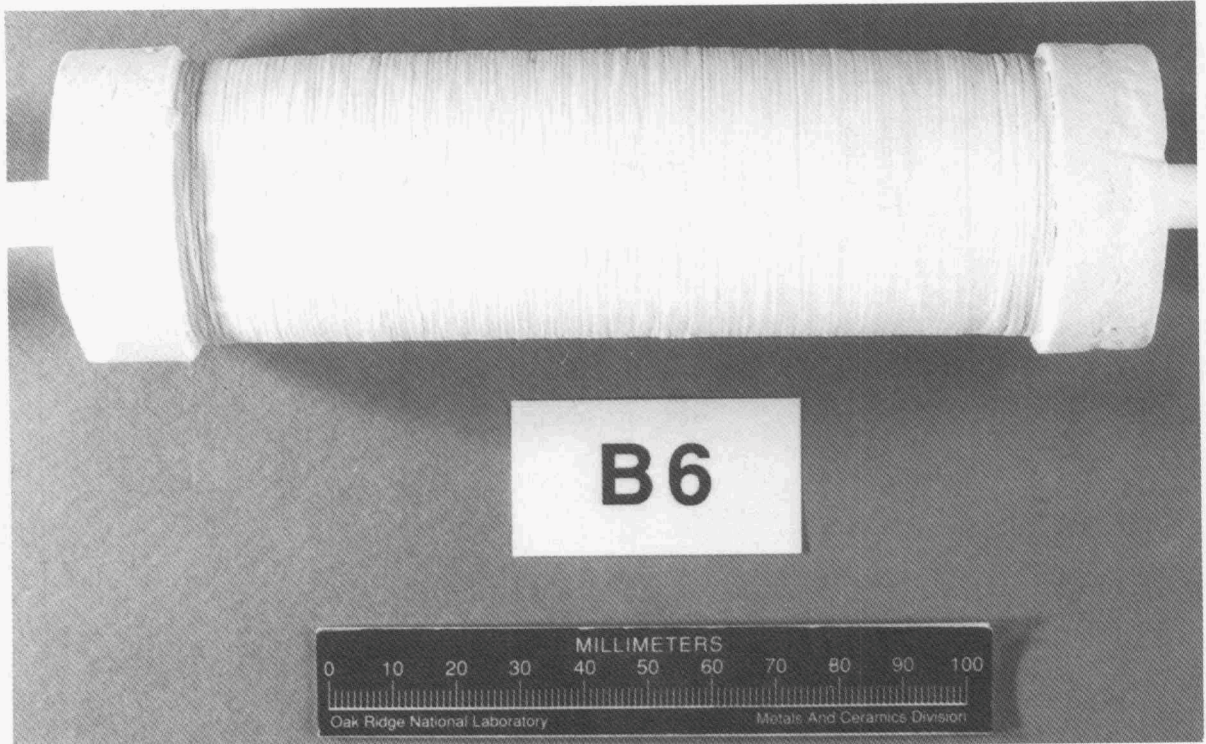
Table 2. Thermal treatments in air and the corrosive atmosphere

Specimen number	Maximum temperature <sup>a</sup> (°C)	Test periods in sequence (h)	Cumulative time (h)	Thermal cycles
<i>Air atmosphere</i>				
A5	1151	100-200-200	500	3
C7	1160	100-200-200	500	3
E9	1147	100-200-200	500	3
G2	1153	100-200-200	500	3
J2	1162	100-200-200	500	3
<i>Corrosive atmosphere</i>				
B6	1153	100-100-100-200	500	4
D18	1162	100-100-100-200	500	4
F15	1147	100-100-100-200	500	4
H3	1153	100-100-100-200	500	4
I2	1162	100-100-100	300 <sup>b</sup>	3
K3	1147	100-100-100	300 <sup>b</sup>	3

<sup>a</sup>Temperature of gas adjacent to specimen.

<sup>b</sup>Exposure terminated because of severe degradation.

YP9768



YP9766

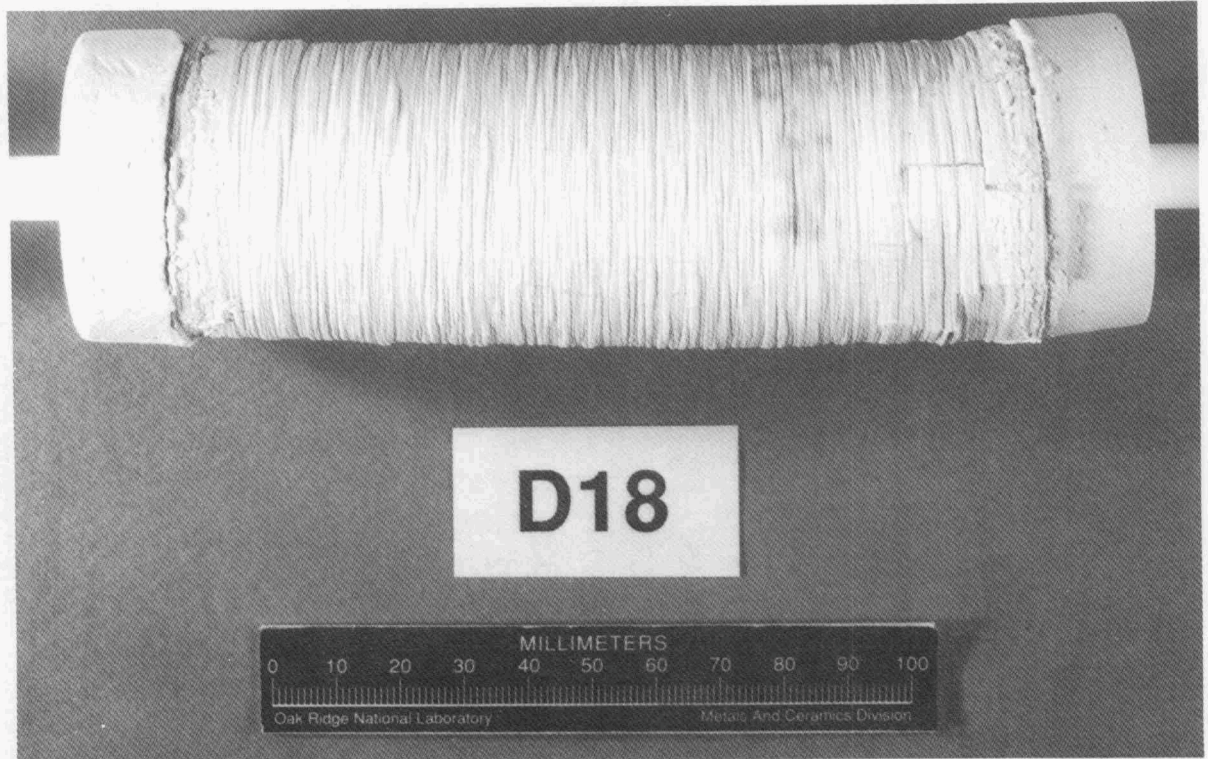
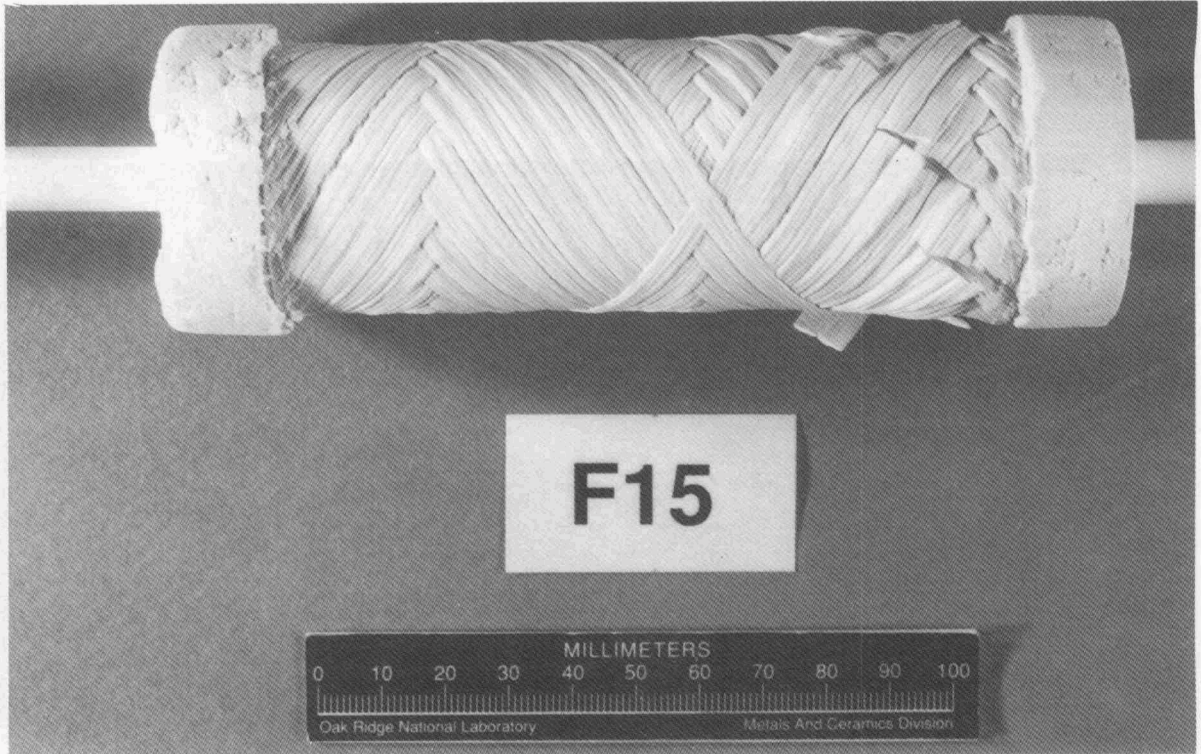


Fig. 5. Hoop-wound specimens after exposure to the corrosive atmosphere for 500 h. B6,  $\text{Al}_2\text{O}_3$  matrix; D18,  $\text{ZrO}_2$  matrix.

YP9765



YP9767



Fig. 6. Helical-wound specimens with  $ZrO_2$  matrices after exposure to the corrosive atmosphere for 500 h.

YP9404



YP9405

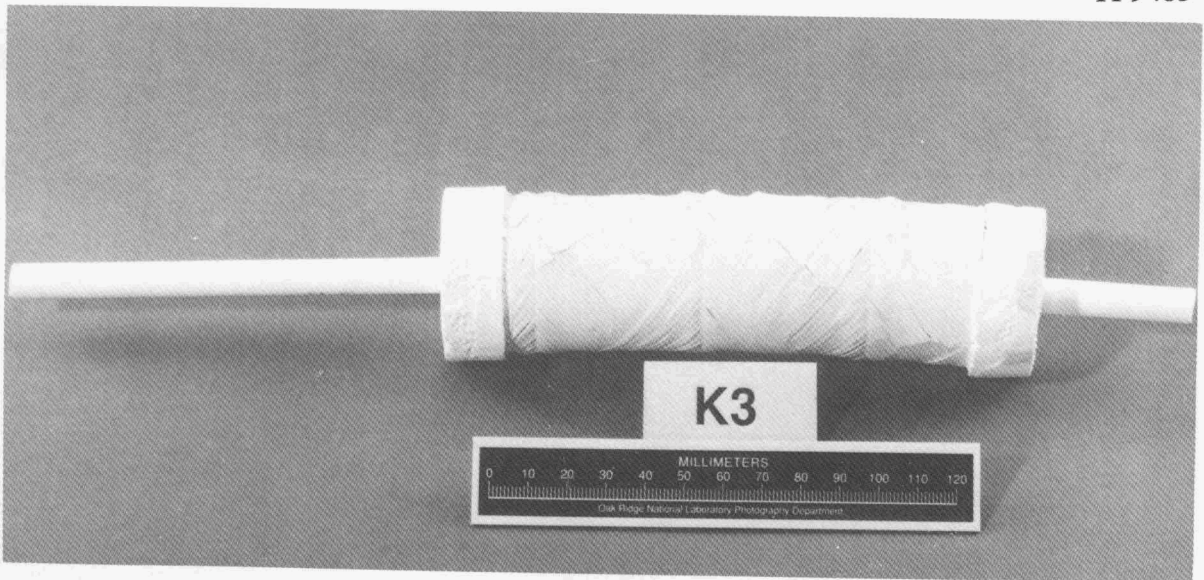


Fig. 7. Helical-wound specimens with  $ZrO_2$  matrices after exposure to the corrosive atmosphere for 300 h. I2,  $SnO_2$  coating; K3,  $ZrO_2$  coating.

Table 3. Temperatures (°C) in three positions in the furnace tubes in air and in the corrosive atmosphere

Position <sup>a</sup> (in.)	Circumferential position (degrees)					
	0		120		240	
	Air	CA <sup>b</sup>	Air	CA <sup>b</sup>	Air	CA <sup>b</sup>
<i>Furnace A, tube 2</i>						
-2	1151	1150	1144	1142	1150	1149
-1	1156	1156	1154	1152	1156	1156
C	1157	1157	1157	1156	1158	1158
+1	1154	1154	1155	1152	1155	1154
+2	1139	1139	1139	1136	1140	1139
<i>Furnace B, tube 3</i>						
-2	1136	1135	1135	1133	1140	1137
-1	1142	1142	1146	1142	1146	1145
C	1143	1143	1148	1146	1144	1142
+1	1135	1135	1143	1141	1137	1135
+2	1115	1115	1127	1124	1118	1114

<sup>a</sup>The "C" position represents the longitudinal midpoint of the specimen, and the numbers represent distance above (-) and below (+) the midpoint. 1 in. = 25 mm.

<sup>b</sup>CA = corrosive atmosphere.

specimens by the furnace. As stated previously, temperatures were lower in end-furnace tubes than in middle tubes (Fig. 2 shows the tube arrangement in the furnaces). In addition, as shown in Table 3, the gradient was more severe in an end-furnace tube (tube 3 in furnace B) compared to a middle tube (tube 2 in furnace A).

## DIMENSIONAL CHANGES

The dimensional changes of specimens heat-treated in the corrosive atmosphere were substantially larger than those of similar specimens heat-treated in air. As with specimens thermally treated in air, eight approximately equally spaced circumferential measurements at each of three longitudinal positions were used to determine the average cumulative diameter changes ( $\Delta D$ ), and four approximately equally spaced measurements were used to determine the average cumulative length changes ( $\Delta L$ ). In Figs. 8–12 the longitudinal positions for diameter measurements are designated C for midpoint and +1 and -1 for positions ~25 mm on either side of the midpoint. Figures 8–12 show that the  $\Delta D$  values for specimens exposed to air ranged from about -0.5 to +0.3%, while Figs. 8–13 show that the  $\Delta D$  values for specimens exposed to the corrosive atmosphere ranged up to +6%. The  $\Delta L$  values showed similar ranges for the two atmospheres. Helical-wound specimen E9, which was tested in air, was not paired with a similar specimen tested in the corrosive atmosphere; therefore, its dimensional changes are compared with hoop-wound specimen A5 in Fig. 10. This comparison does not clearly favor one type of winding method over the other. Specimen I2, which was not paired with a similar specimen tested in air, had substantial dimensional changes after 300 h (Fig. 13). Unfortunately, comparisons based on dimensional changes among specimens exposed to the corrosive atmosphere for 500 h in Figs. 8, 9, 11, and 12 do not reveal a clear choice between  $\text{Al}_2\text{O}_3$  and  $\text{ZrO}_2$  matrices nor between hoop and helical winding.

ORNL-DWG 90-17134

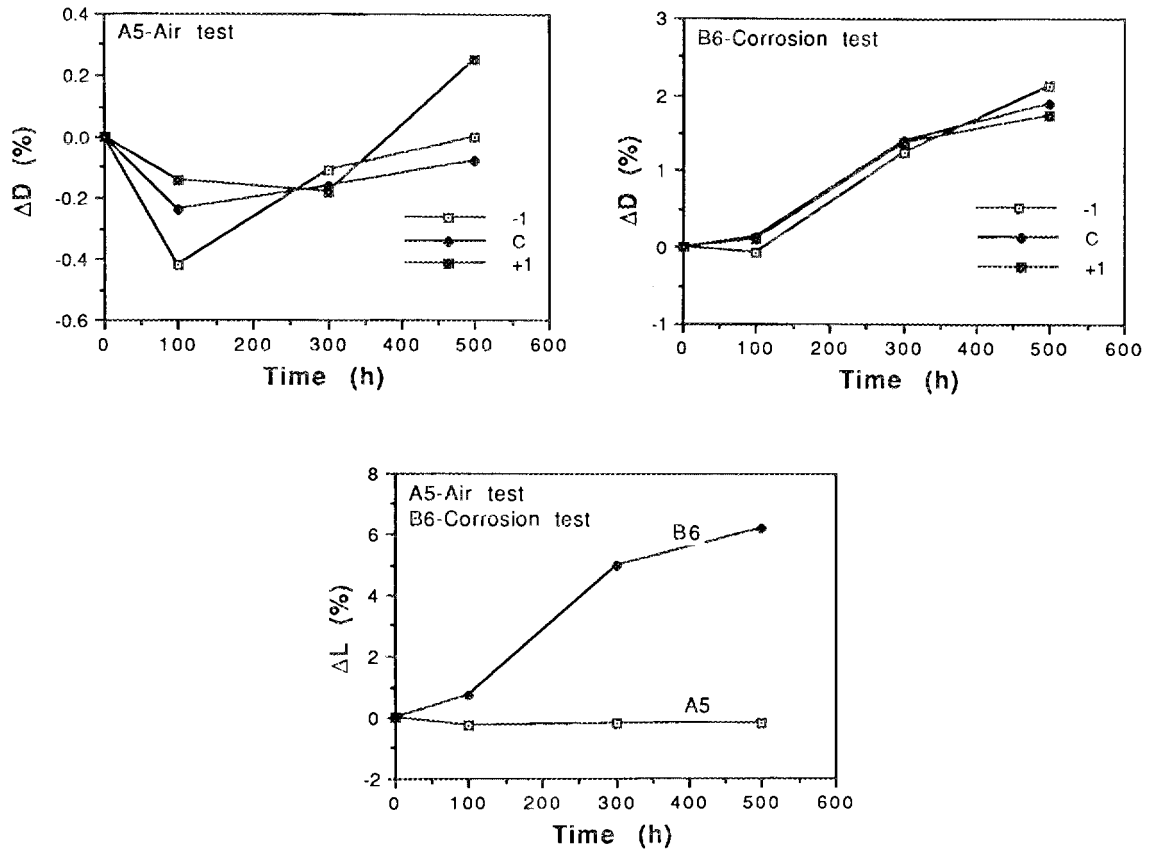


Fig. 8. Dimensional changes in hoop-wound specimens A5 and B6 with  $Al_2O_3$  matrices.

ORNL-DWG 90-17135

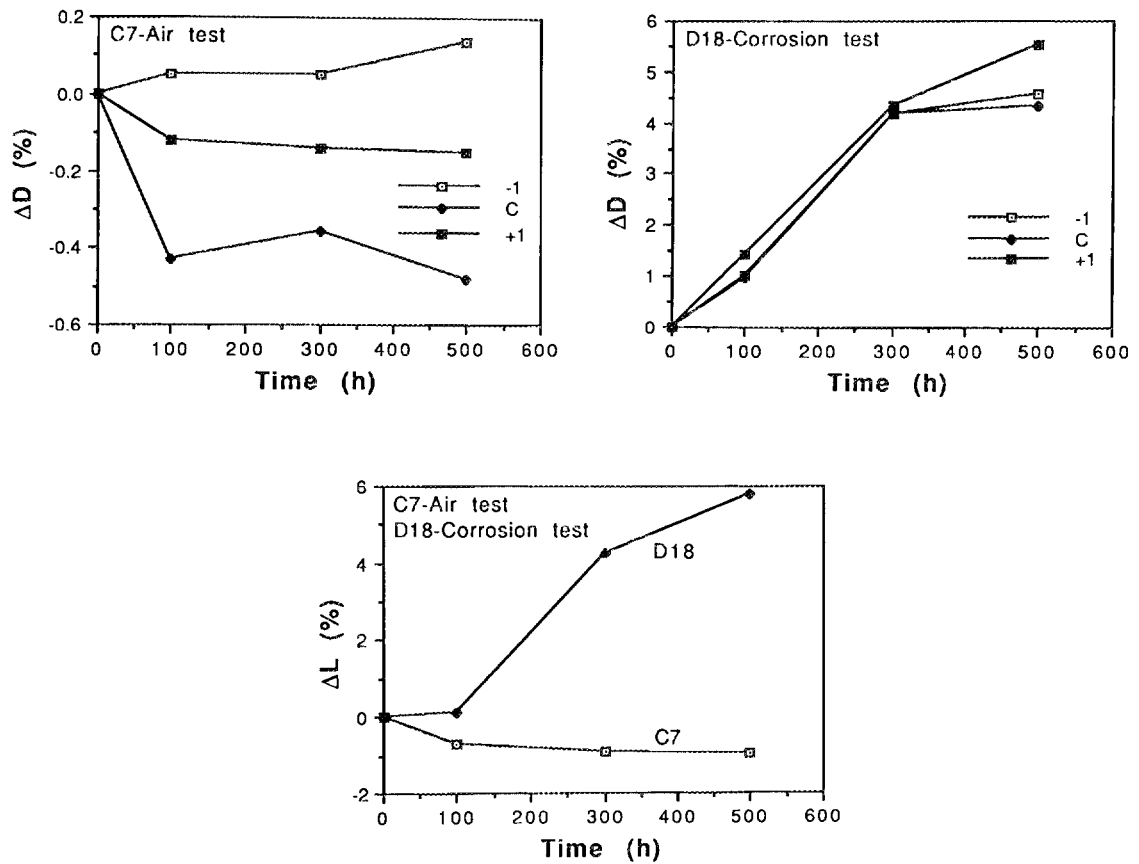


Fig. 9. Dimensional changes in hoop-wound specimens C7 and D18 with ZrO<sub>2</sub> matrices.

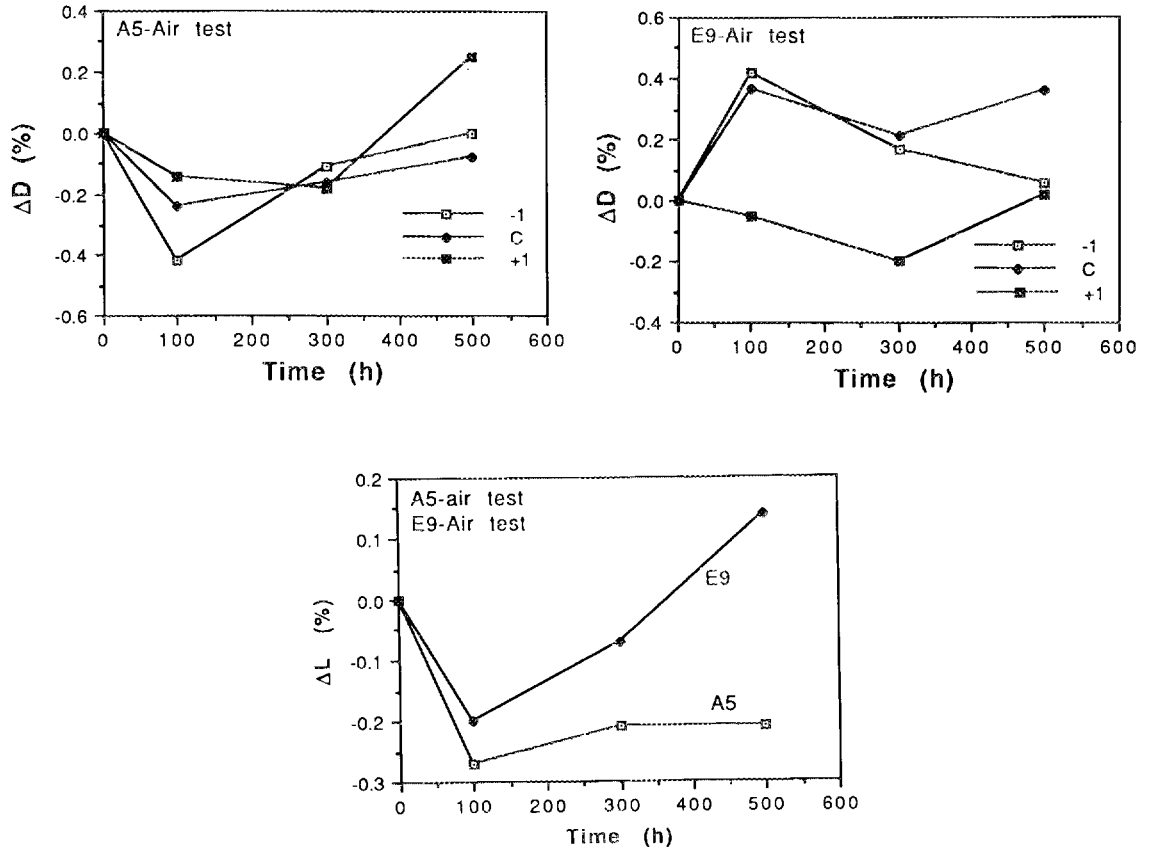


Fig. 10. Dimensional changes in hoop-wound (A5) and helical-wound (E9) specimens with  $Al_2O_3$  matrices tested in air.

ORNL-DWG 90-17137

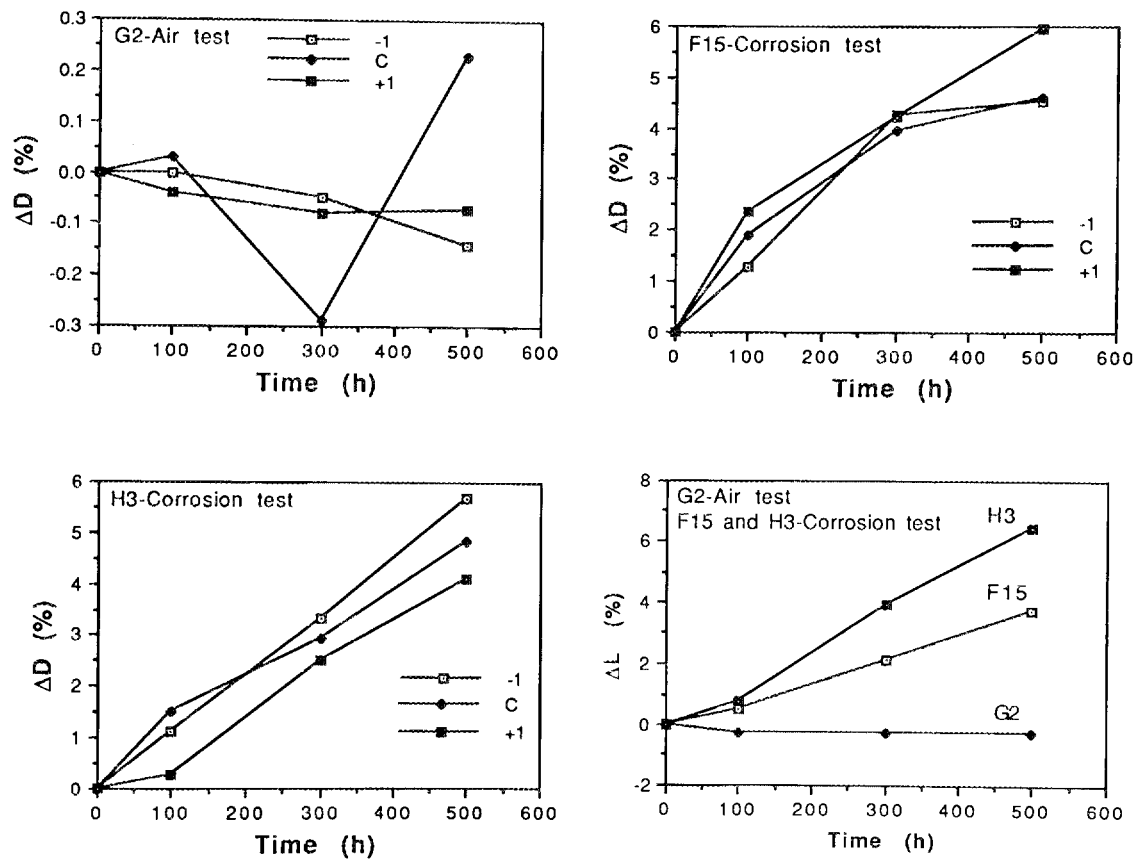


Fig. 11. Dimensional changes in helical-wound specimens G2, F15, and H3 with  $ZrO_2$  matrices.

ORNL-DWG 90-17138

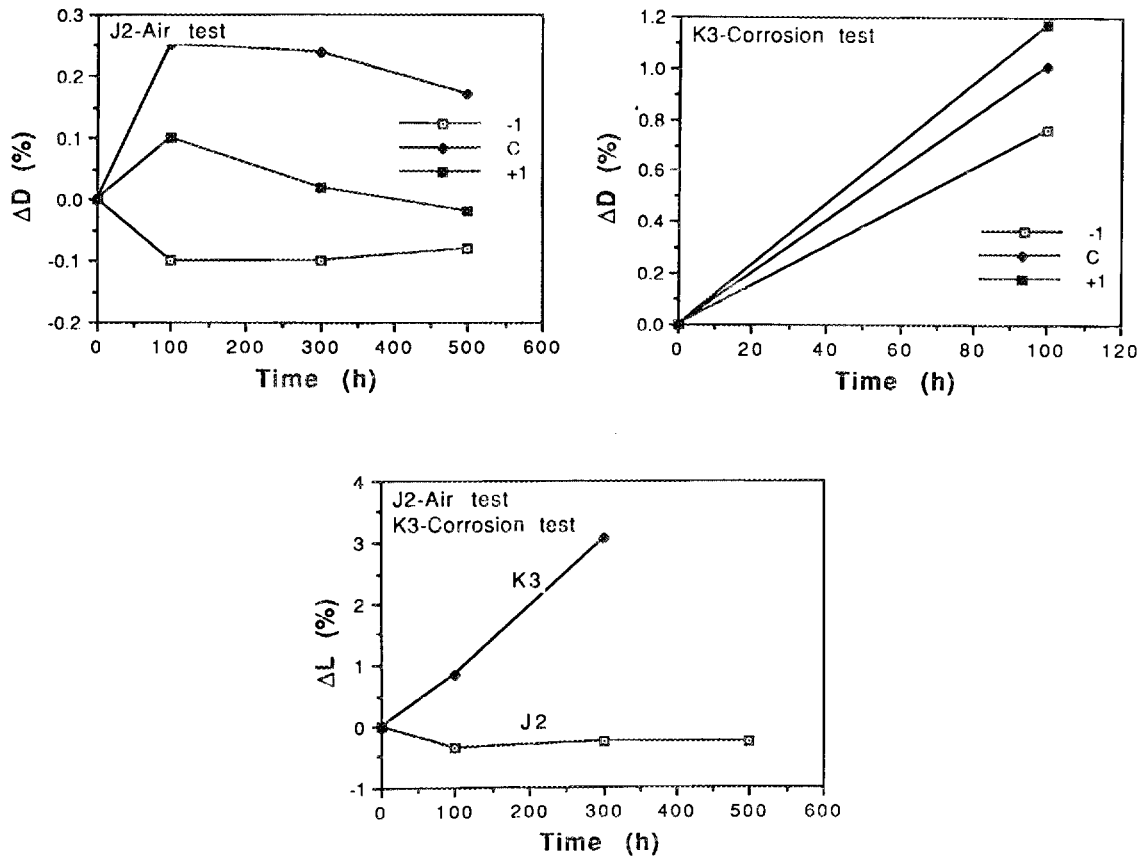


Fig. 12. Dimensional changes in helical-wound specimens J2 and K3 with ZrO<sub>2</sub> matrices.

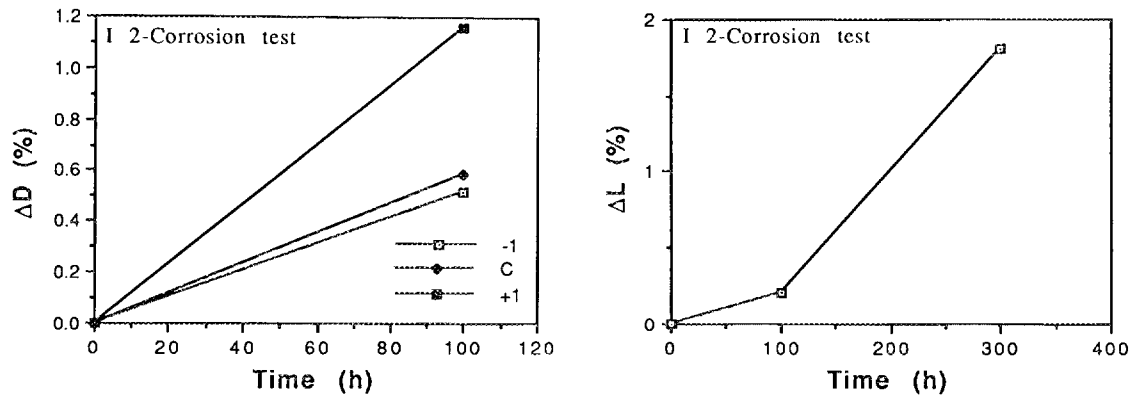


Fig. 13. Dimensional changes in helical-wound specimen I2 with a ZrO<sub>2</sub> matrix.

#### OPTICAL MICROSCOPY

Optical micrographs of specimens tested in air (Figs. 14–16) showed pores, cracks, and large voids in the matrix, which were probably present in the as-fabricated condition. Voids were usually filled with epoxy, the material used to prepare the specimen for examination. The cracks in the matrices were always perpendicular to the uncracked filaments, indicating that the filaments substantially strengthened the composites. Optical micrographs of samples from the most severely damaged regions of specimens tested in the corrosive atmosphere also revealed structural degradation (Figs. 17–22). Some had exfoliated layers that appear as wide cracks in the optical micrographs. Figure 17(a) shows a cross section perpendicular to the filaments of a hoop-wound specimen (B6) with an Al<sub>2</sub>O<sub>3</sub> matrix. The dark-gray regions are voids filled with epoxy. Cracks such as that in the lower part of the picture probably formed by linking voids under thermal stresses. Figure 17(b) shows voids in the matrix in regions of low filament population. A cracked and porous layer of material about 50  $\mu\text{m}$  thick at the surface contained no filaments.

YP11567

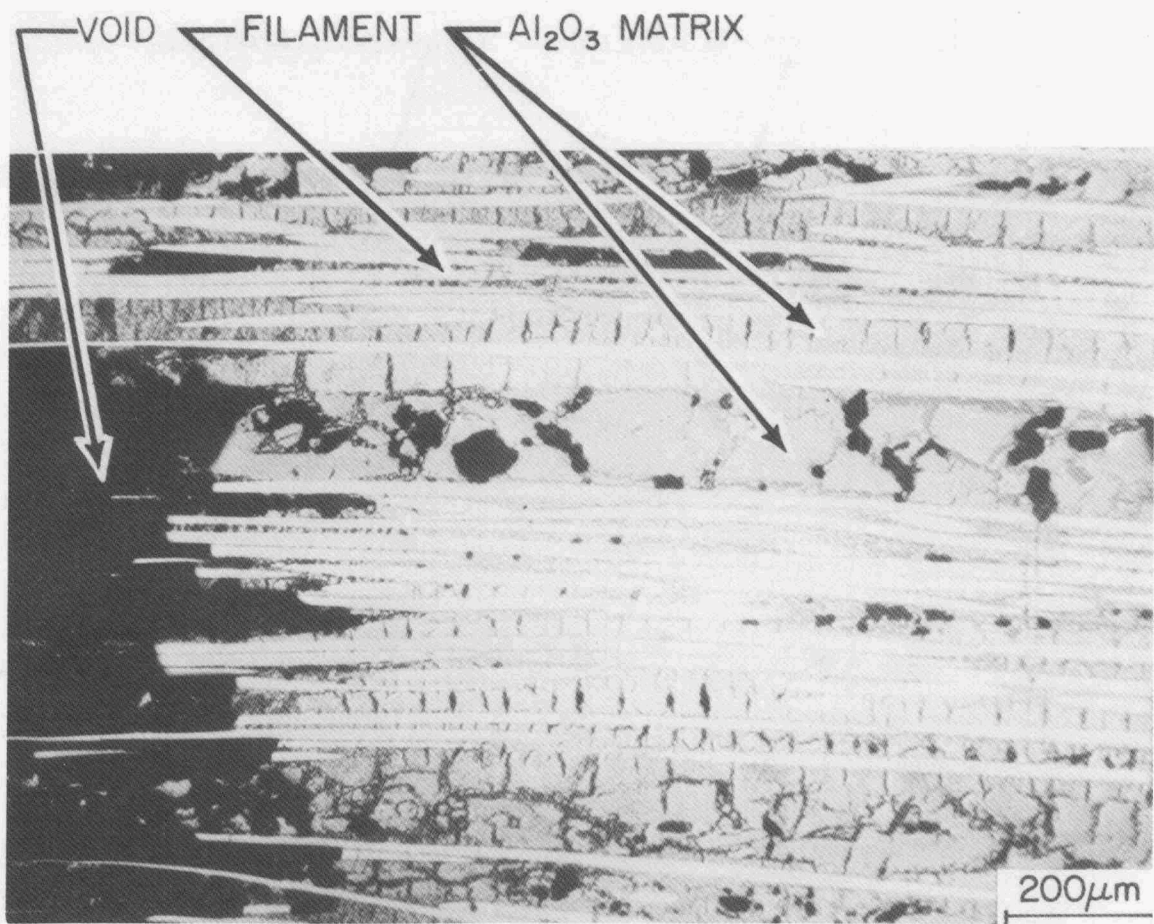


Fig. 14. Specimen A5 after testing in air.

YP11566

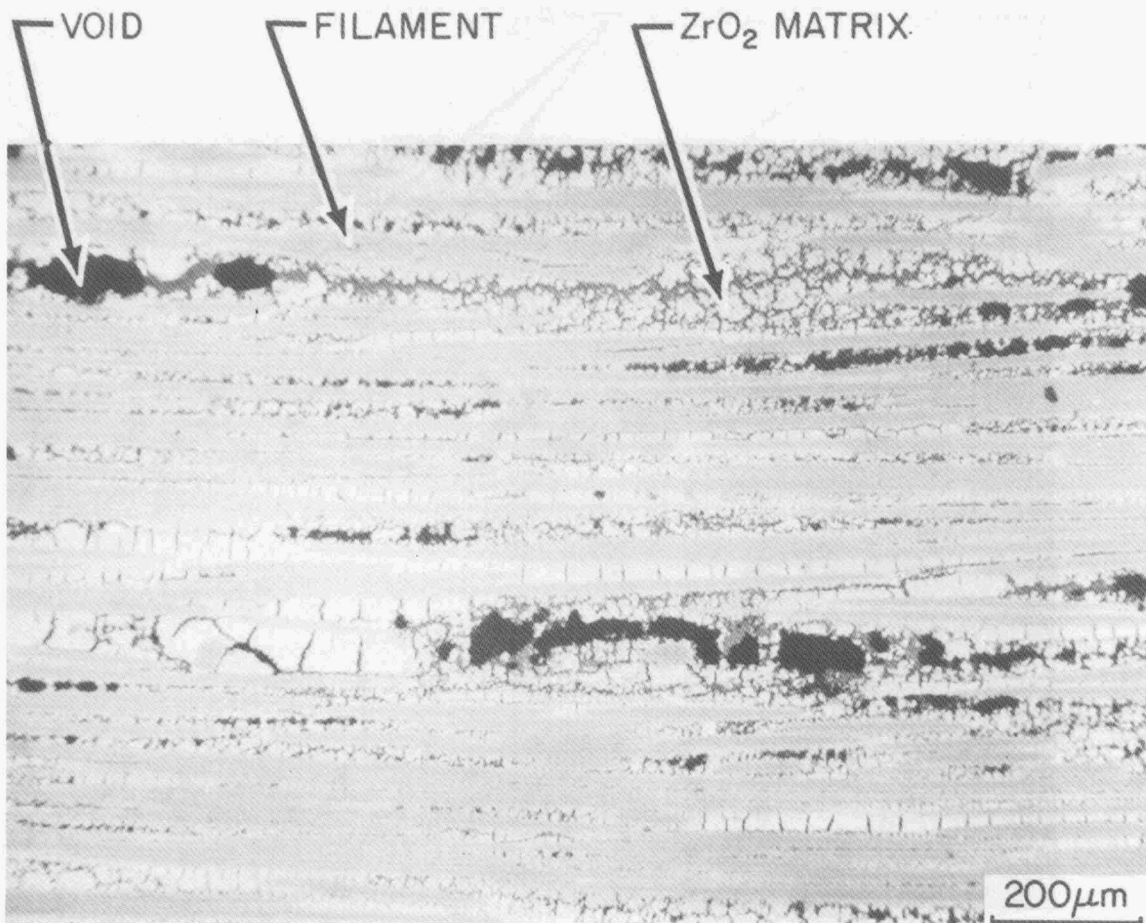


Fig. 15. Specimen C7 after testing in air.

YP11573

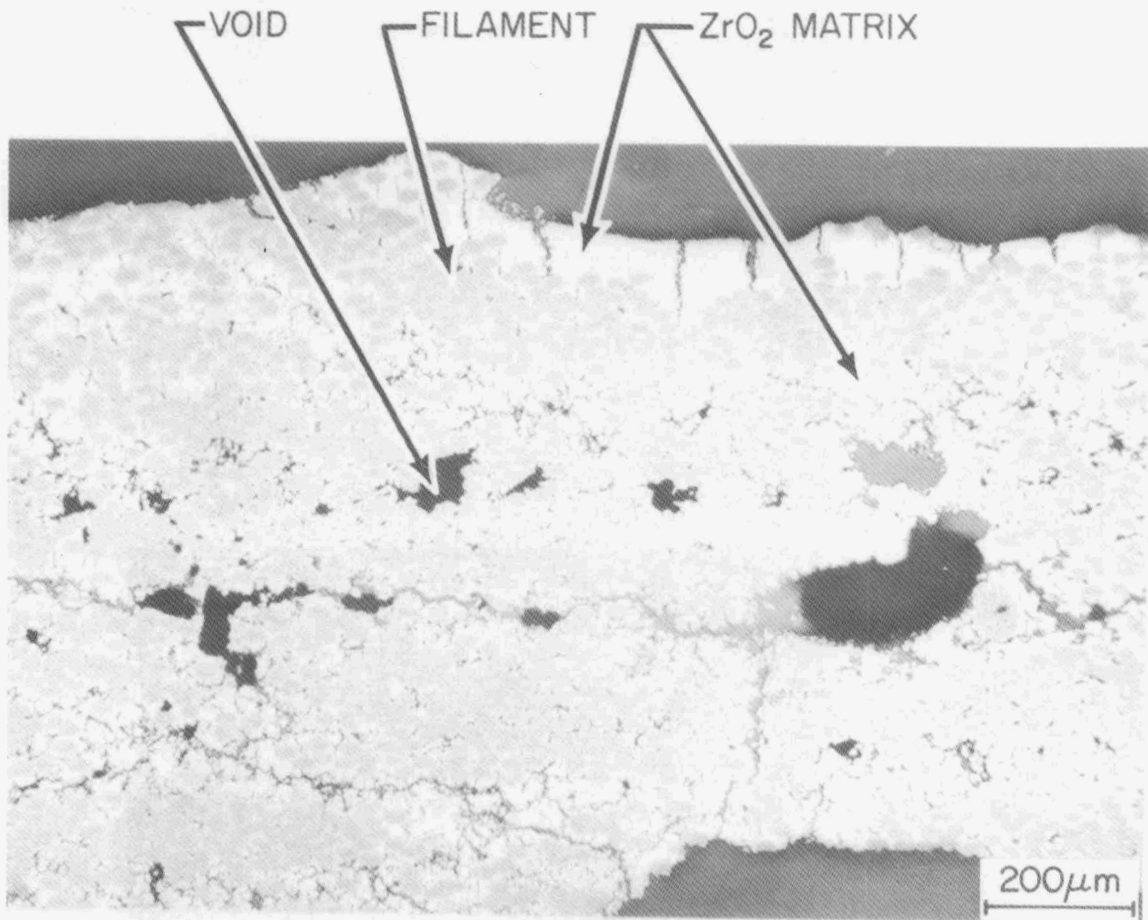


Fig. 16. Specimen G2 after testing in air.

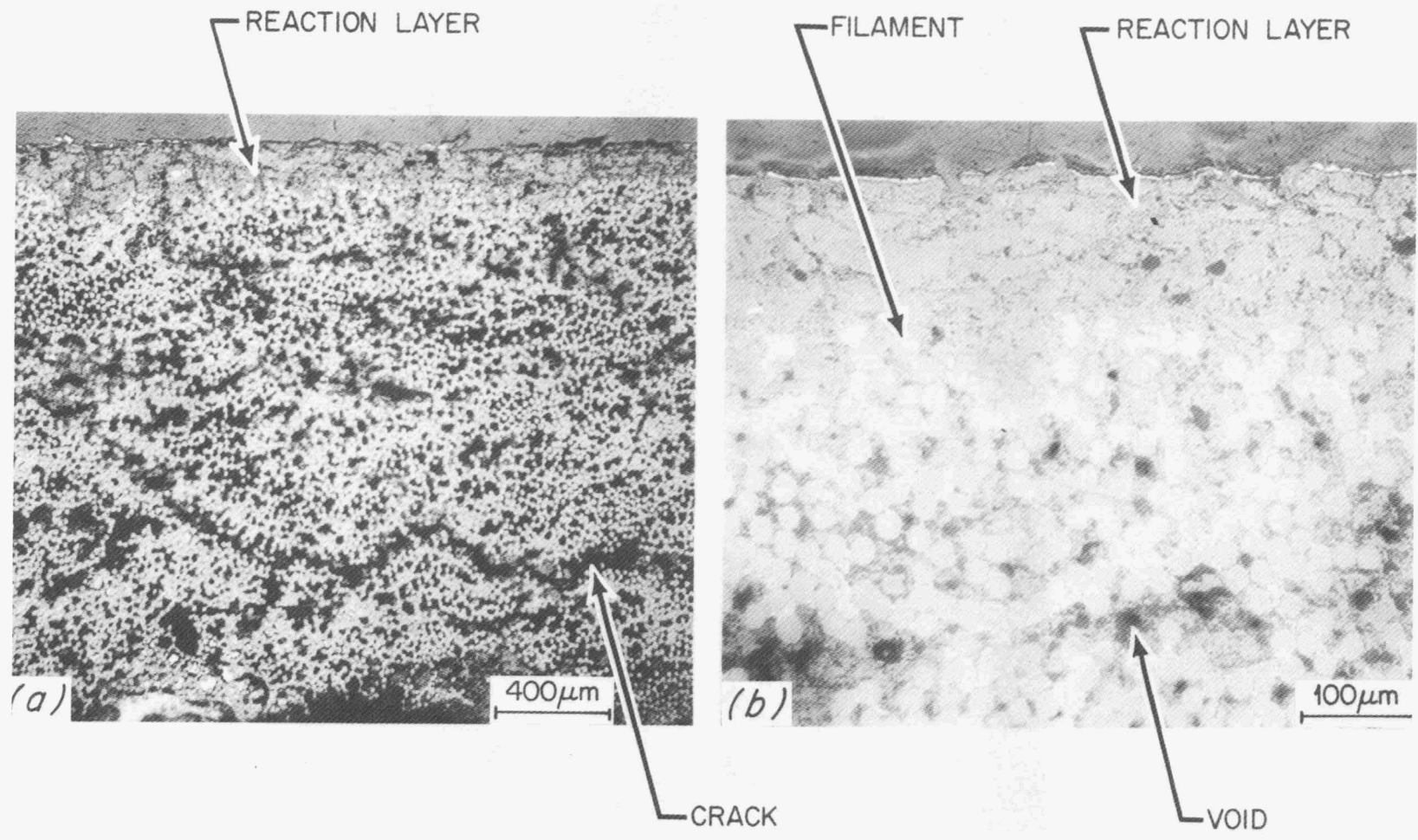


Fig. 17. Specimen B6 after corrosion testing.

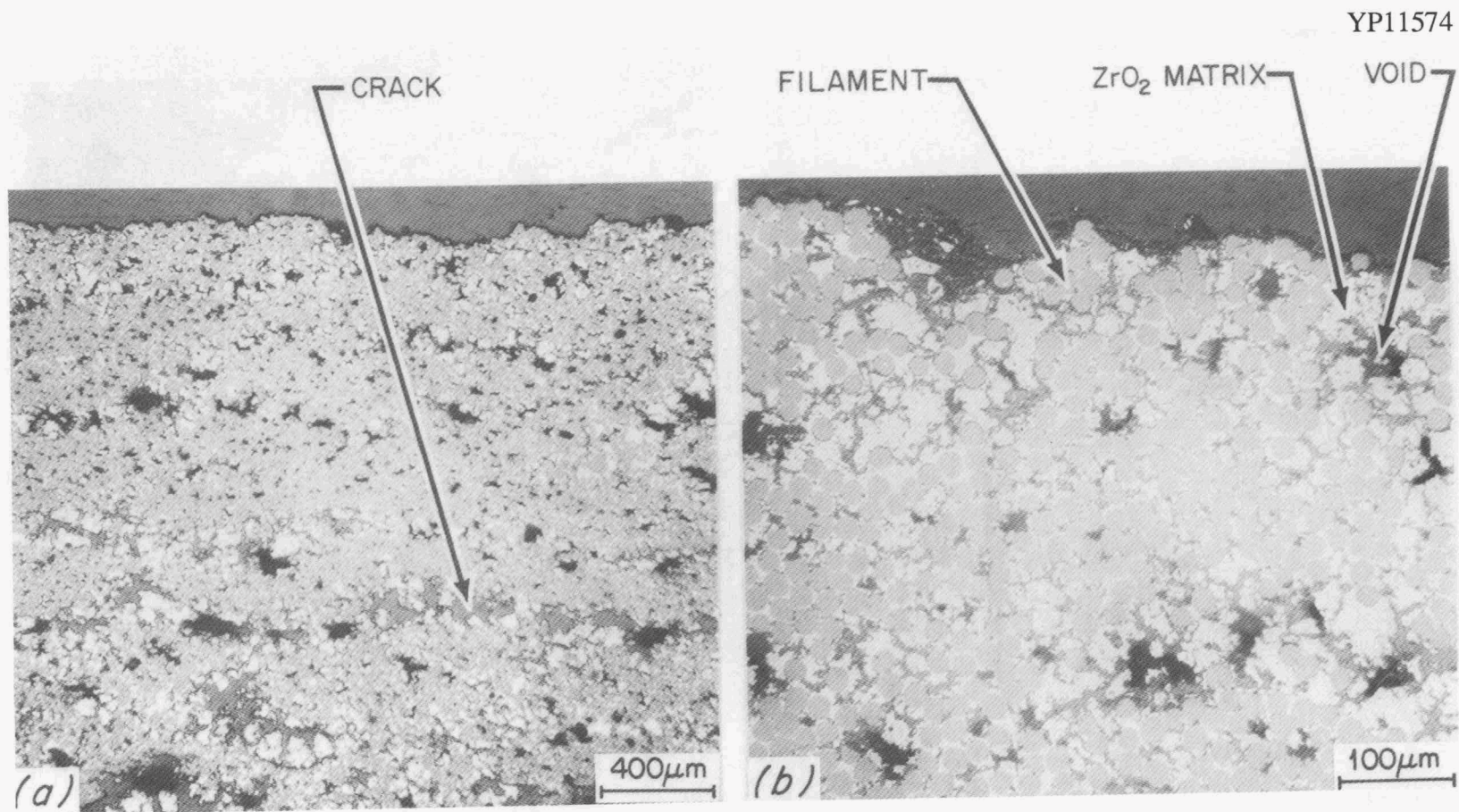


Fig. 18. Specimen D18 after corrosion testing.

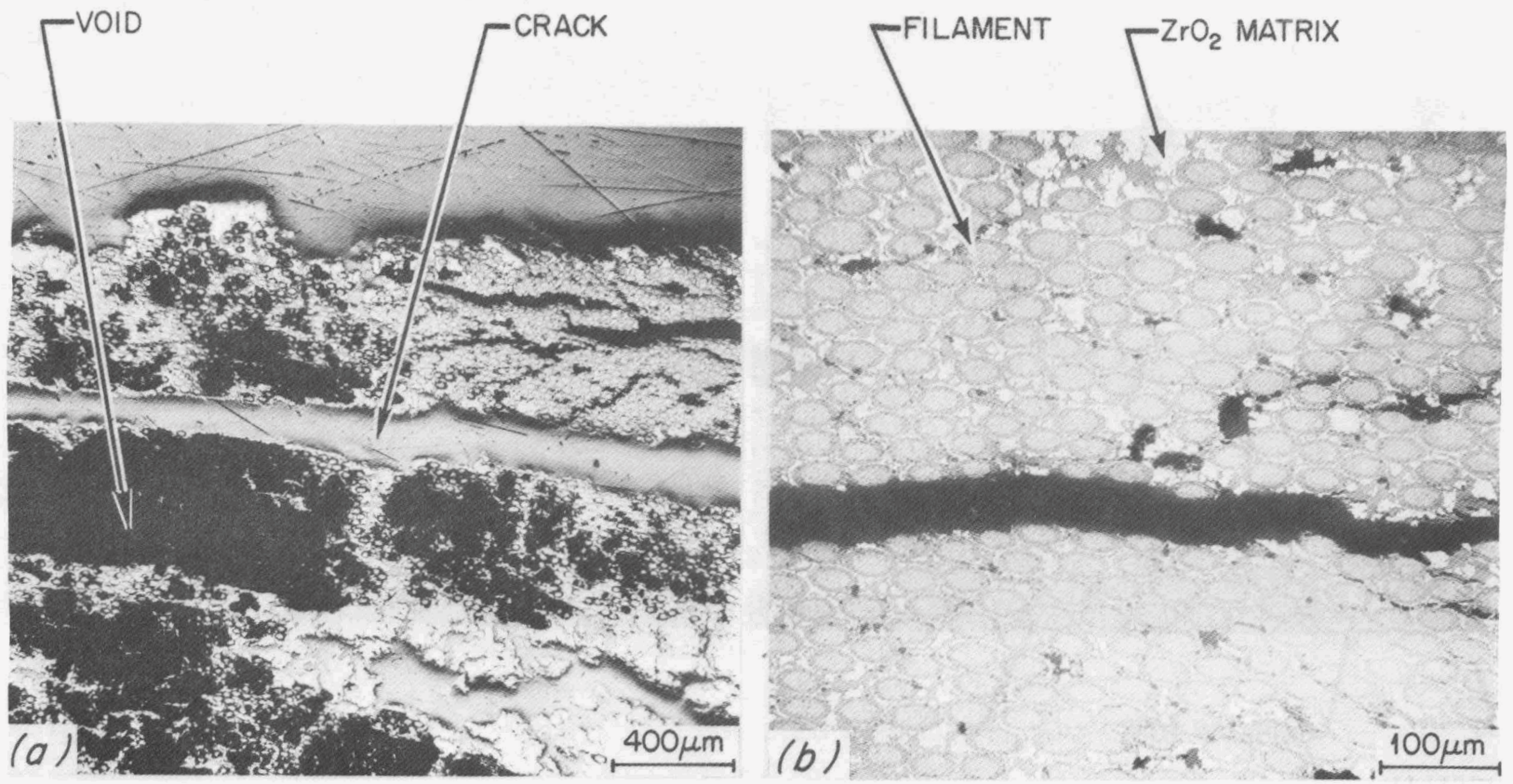


Fig. 19. Specimen F15 after corrosion testing.

YP11570

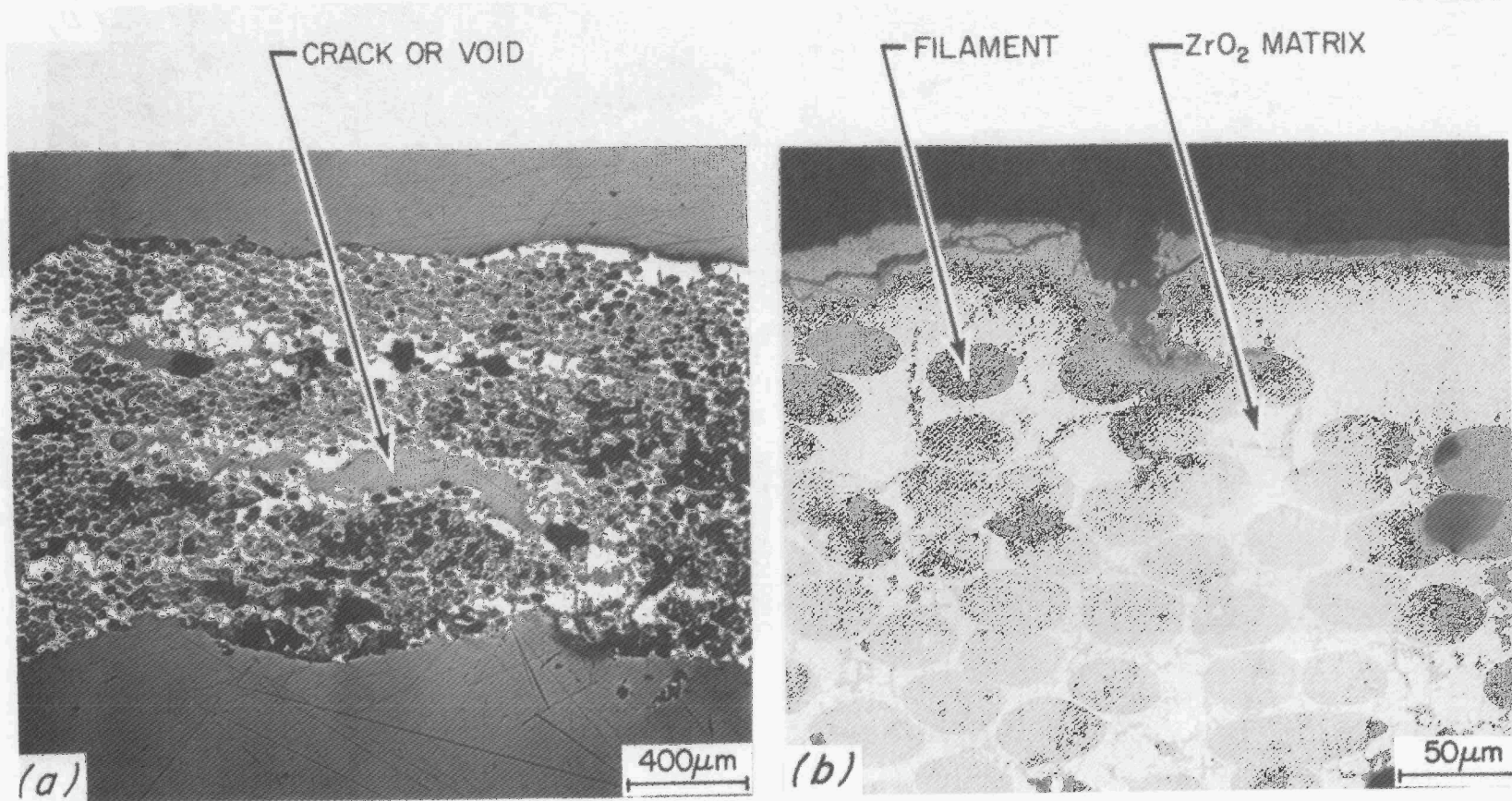


Fig. 20. Specimen H3 after corrosion testing.

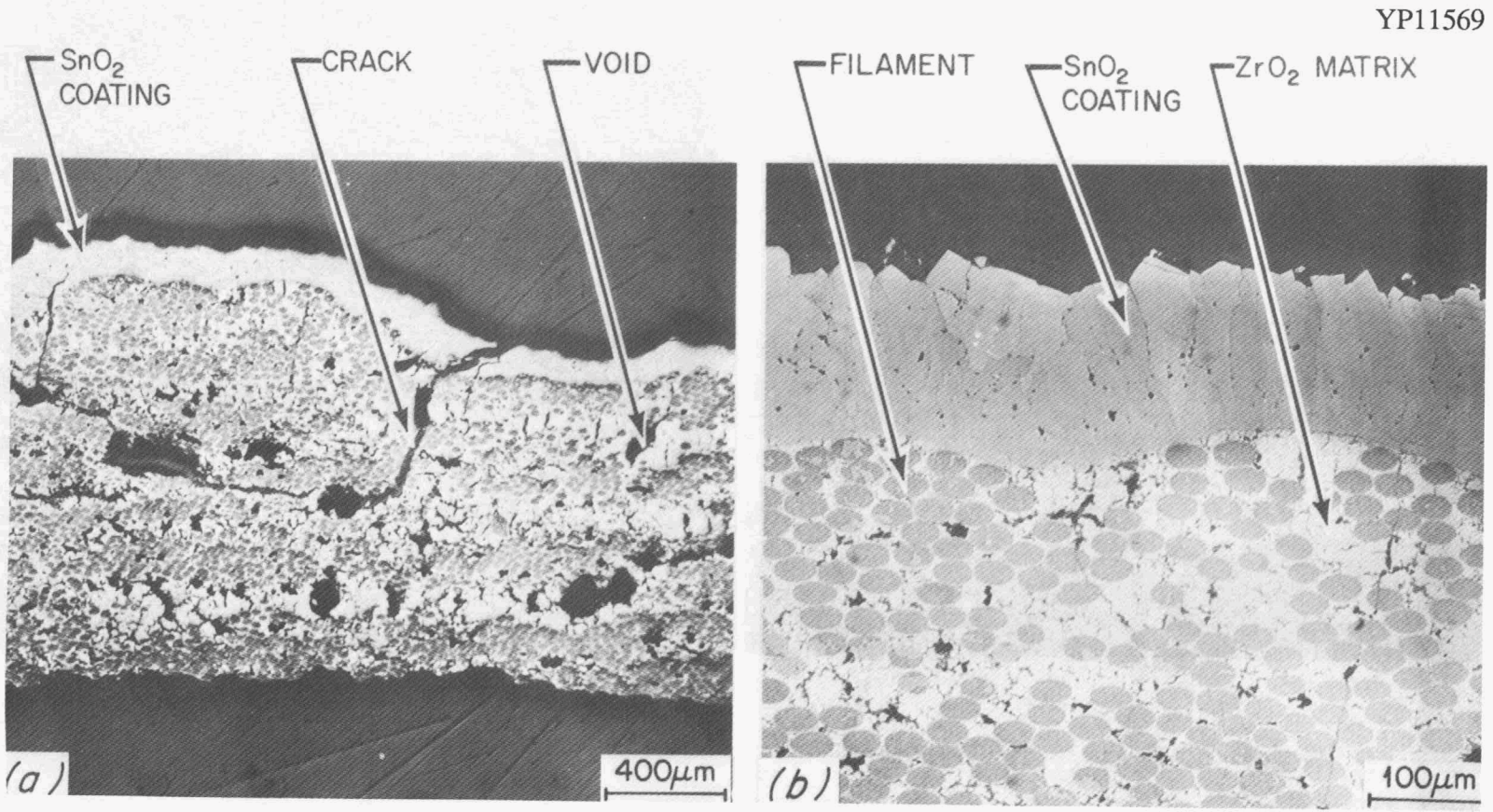


Fig. 21. Specimen 12 after corrosion testing.

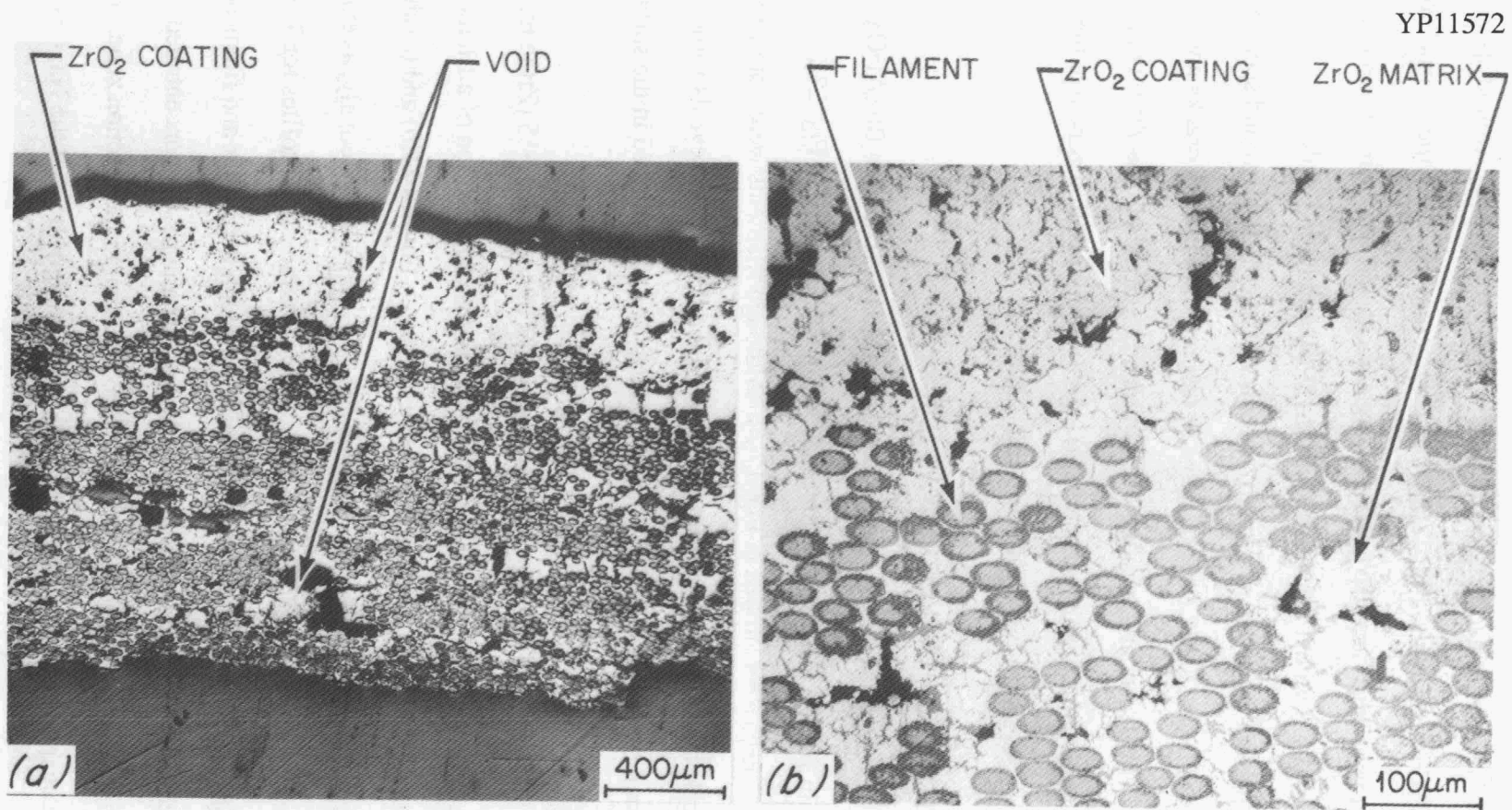


Fig. 22. Specimen K3 after corrosion testing.

Figure 18(a) shows cracks and voids in the structure of a hoop-wound specimen (D18) with a  $\text{ZrO}_2$  matrix, and Fig. 18(b) shows numerous cracks in the matrix. Regions of low filament population are also evident. Large cracks and voids are shown in a helical-wound specimen (F15) with a  $\text{ZrO}_2$  matrix [Figs. 19(a) and (b)]. In addition, an apparent reaction zone is present at the filament/matrix interface. Other helical-wound specimens with  $\text{ZrO}_2$  matrices in Figs. 20–22 (H3, I2, and K3, respectively) exhibit cracks and voids in the matrix. The dense  $\text{SnO}_2$  coating on specimen I2 and the porous  $\text{ZrO}_2$  coating on specimen K3 are evident in Figs. 21(a) and 22(a). An apparent reaction zone like that mentioned above is present in specimen K3 in Fig. 22(b).

#### ELECTRON MICROPROBE ANALYSIS

The results of electron microprobe analysis of specimen B6 ( $\text{Al}_2\text{O}_3$  matrix) are shown in Fig. 23. The backscattered electron (BSE) image in Fig. 23(a) shows the region near the surface mentioned in Fig. 17(b). Although filaments were not visible in the optical micrograph of the surface layer in Fig. 17(b), the BSE image reveals some filaments. The elemental dot map in Fig. 23(b) shows that Na was concentrated in the surface layer along with a high concentration of Al (not shown in Fig. 23).

The electron microprobe analysis results of specimen F15 ( $\text{ZrO}_2$  matrix) are shown in Fig. 24. The BSE image [Fig. 24(a)] shows the cross section of a filament, the cracked  $\text{ZrO}_2$  matrix, and the reaction zone at the interface. Figures 24(b) and (c) show that  $\text{Al}_2\text{O}_3$  and  $\text{ZrO}_2$  were concentrated in the filaments and matrix, respectively, as expected. Figures 24(d) and (e) show the results of concentration line profiles for Ti and Na. The straight light line shows the path of analysis through the matrix and filament, and the saw-toothed lines show the concentration changes. Titanium was concentrated in the reaction zone and Na was concentrated in the matrix adjacent to the reaction zone. The presence of Ti is unexplained (none was detected in other specimens); but the Na, no doubt, was

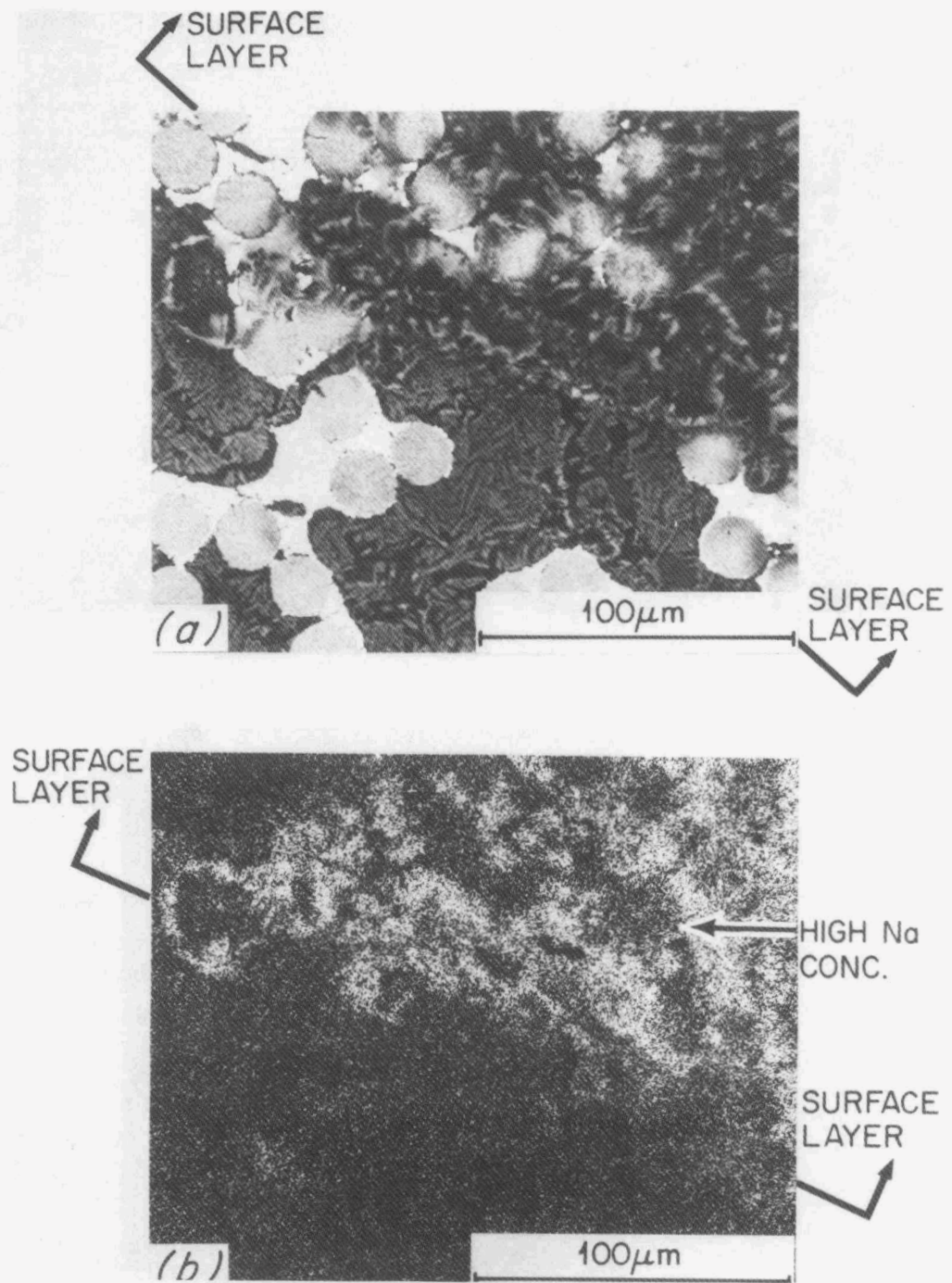


Fig. 23. Electron microprobe analysis of specimen B6 after corrosion testing.

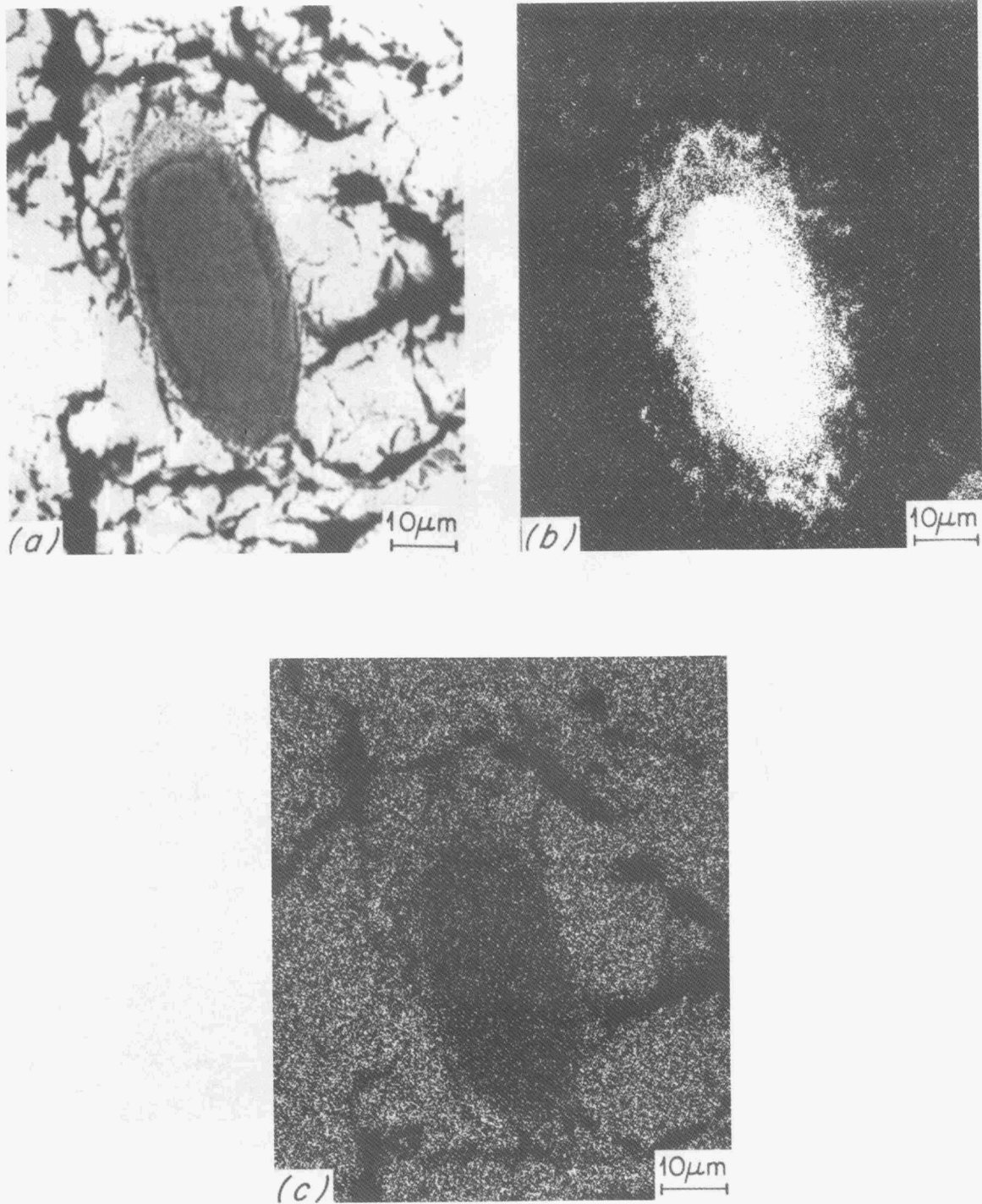


Fig. 24. Electron microprobe analysis of specimen F15 after corrosion testing.

YP11578

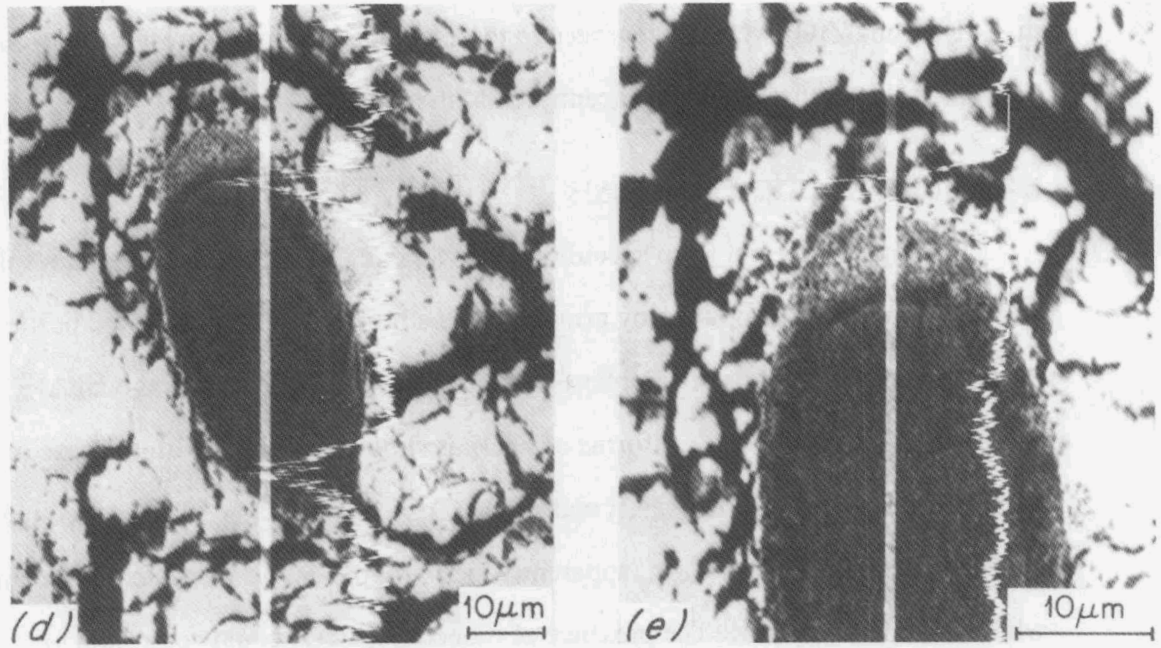


Fig. 24. (Continued)

derived from the corrosion atmosphere. Sodium carbonate apparently migrated through the  $\text{ZrO}_2$  matrix to react with the  $\text{Al}_2\text{O}_3$ -20 wt %  $\text{ZrO}_2$  filaments, indicating that Na forms compounds more readily with  $\text{Al}_2\text{O}_3$  than with  $\text{ZrO}_2$  at the temperatures used in these tests.

Figure 25 shows similar results for specimen K3. The BSE image in Fig. 25(a) clearly shows a reaction layer at the matrix/filament interface. Figures 25(b) and (c) show that  $\text{Al}_2\text{O}_3$  and  $\text{ZrO}_2$  were concentrated in the filaments and matrix, respectively, and Fig. 25(d) shows that Na was concentrated at the interface.

#### X-RAY DIFFRACTION ANALYSIS

Samples were cut from specimens tested in air and in the corrosive atmosphere. These were reduced to powder by grinding with a boron carbide mortar and pestle. X-ray diffraction patterns of samples exposed to air revealed only hexagonal  $\text{Al}_2\text{O}_3$  and monoclinic and tetragonal forms of  $\text{ZrO}_2$  as shown in Table 4. In the case of specimen A5, which had an  $\text{Al}_2\text{O}_3$  matrix, the  $\text{ZrO}_2$  phases apparently were contained in the filaments. Similarly,  $\text{Al}_2\text{O}_3$  (apparently in the filaments) was detected in specimen C7, which had a  $\text{ZrO}_2$  matrix. The presence of monoclinic  $\text{ZrO}_2$  could contribute to dimensional instability in the specimens because of a volume change of about 9% occurring during transformations between the monoclinic and tetragonal forms. On the other hand, uniformly distributed particles of tetragonal  $\text{ZrO}_2$  can toughen a mostly cubic  $\text{ZrO}_2$  material by transforming to less dense monoclinic under stress. The resulting compressive stresses in the matrix tend to stop crack propagation. In the case of specimens heat-treated in air, degradation was minimal, suggesting that destructive transformations did not occur.

Specimens exposed to the corrosive atmosphere contained one or more sodium aluminate compounds (Table 4). The X-ray data base<sup>4</sup> used to identify these compounds contained  $\text{Na}_2\text{O}\cdot\text{Al}_2\text{O}_3$ ,  $\text{Na}_2\text{O}\cdot 11 \text{Al}_2\text{O}_3$ ,  $\text{Na}_2\text{O}\cdot 7 \text{Al}_2\text{O}_3$ , and  $\text{Na}_2\text{O}\cdot 5 \text{Al}_2\text{O}_3$ . For many

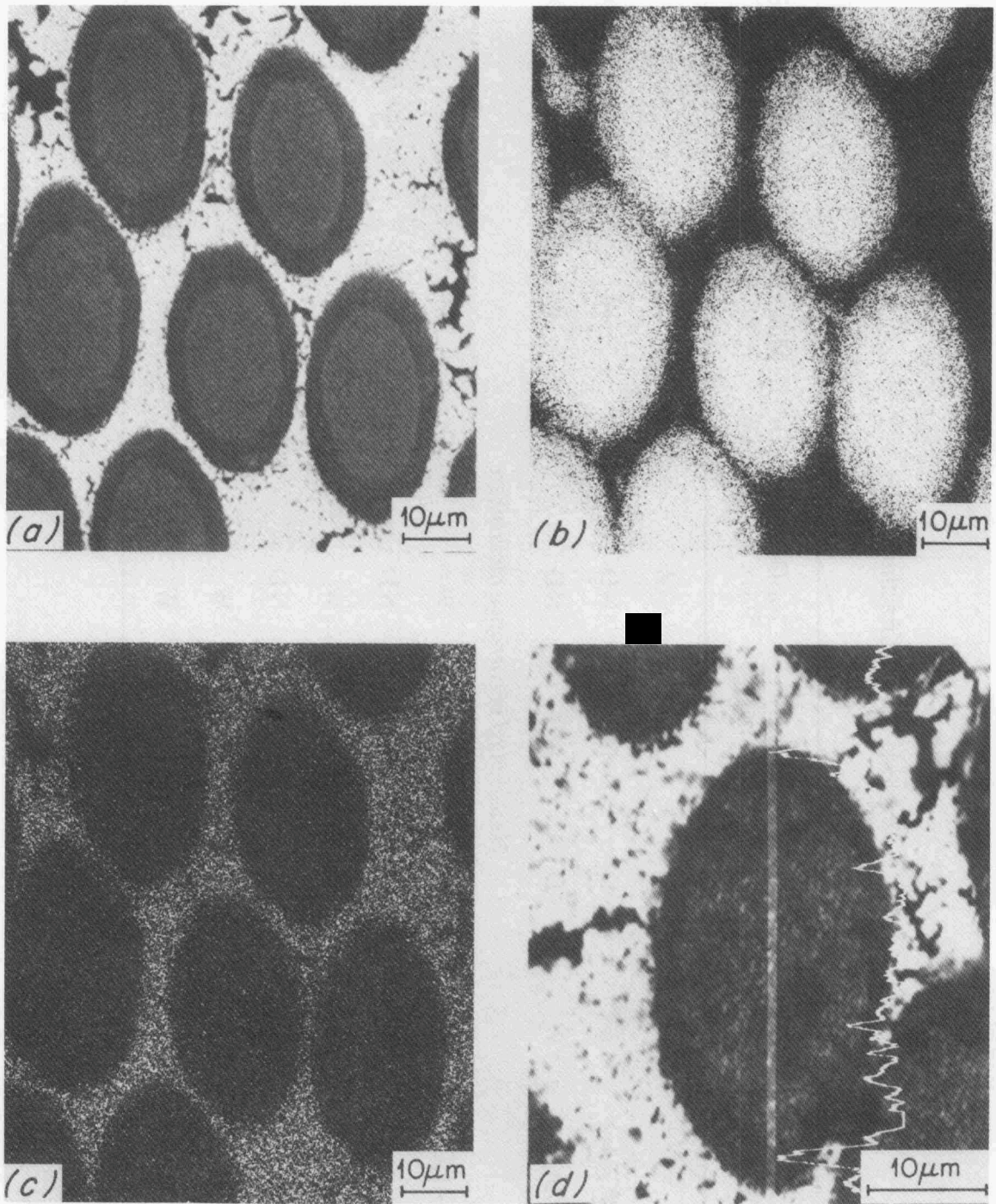


Fig. 25. Electron microprobe analysis of specimen K3 after corrosion testing.

Table 4. X-ray diffraction results

Sample	Matrix	Al <sub>2</sub> O <sub>3</sub>	Na <sub>2</sub> O• 11 Al <sub>2</sub> O <sub>3</sub>	Na <sub>2</sub> O• 7 Al <sub>2</sub> O <sub>3</sub>	Na <sub>2</sub> O• 5 Al <sub>2</sub> O <sub>3</sub>	Na <sub>2</sub> O• Al <sub>2</sub> O <sub>3</sub>	Monoclinic ZrO <sub>2</sub>	Tetragonal ZrO <sub>2</sub>	Cubic ZrO <sub>2</sub>
<i>Heat-treated in air</i>									
A5	Al <sub>2</sub> O <sub>3</sub>	S	ND	ND	ND	ND	W	M	ND
C7	ZrO <sub>2</sub>	W	ND	ND	ND	ND	W-	S	ND
<i>Heat-treated in corrosive atmosphere</i>									
B6	Al <sub>2</sub> O <sub>3</sub>	M	W+	ND	W+	ND	M-	M	M
D18	ZrO <sub>2</sub>	ND	ND	ND	ND	W-	W-	W	S+
F15	ZrO <sub>2</sub>	ND	ND	ND	W	ND	W-	ND	S
H3	ZrO <sub>2</sub>	ND	ND	ND	ND	ND	W-	W-	S
I2	ZrO <sub>2</sub>	W-	ND	ND	W	ND	W-	S	ND
K3	ZrO <sub>2</sub>	ND	ND	ND	W-	W-	W	W	S

Legend: S = strong intensity  
M = medium intensity  
W = weak intensity  
ND = not detected

years there was much controversy over the number, composition, and stability ranges of phases in the  $\text{Na}_2\text{O}-\text{Al}_2\text{O}_3$  system. A recent phase diagram<sup>5</sup> of  $\text{Na}_2\text{O}\cdot\text{Al}_2\text{O}_3-\text{Al}_2\text{O}_3$  shows two intermediate compounds at  $\text{Na}_2\text{O}:\text{Al}_2\text{O}_3$  ratios of 1:11 and in the range 1:5 to 1:7. The theoretical density<sup>6</sup> of  $\text{Na}_2\text{O}\cdot 11 \text{ Al}_2\text{O}_3$  is reported to be  $3.26 \text{ g/cm}^3$ . This value was obtained by sintering at  $1750^\circ\text{C}$ .<sup>6</sup> Both the original sintering temperature for the composites in this work and the temperature of about  $1150^\circ\text{C}$  in the corrosion tests were much lower than  $1750^\circ\text{C}$ . Presumably the densities of the other compounds would be lower because of their higher  $\text{Na}_2\text{O}$  contents. Therefore, a volume expansion of 15% or more probably occurred when  $\text{Na}_2\text{O}$ , which was derived from  $\text{Na}_2\text{CO}_3$ , reacted with  $\text{Al}_2\text{O}_3$  (density of  $3.9 \text{ g/cm}^3$ ) in the matrix or filament to form new compounds. The X-ray diffraction data did not reveal the presence of sodium zirconate ( $\text{Na}_2\text{O}\cdot\text{ZrO}_2$ ), indicating that this compound is not readily formed under the conditions of this test.

## DISCUSSION

Monoclinic, tetragonal, and cubic forms of  $\text{ZrO}_2$  were identified. The cubic form was the dominant phase in four specimens. The structural stability of continuous-filament ceramic matrix composites depends upon the properties of the components, in particular, the coefficients of thermal expansion (CTE) and the mechanical properties of filament and matrix. The CTE of hexagonal  $\text{Al}_2\text{O}_3$  is about  $8.3 \times 10^{-6}/^\circ\text{C}$  over the temperature range of this study, while that of  $\text{ZrO}_2$  could vary considerably depending on the amounts of monoclinic, tetragonal, and cubic phases present. The value would range from about  $8 \times 10^{-6}/^\circ\text{C}$  for all monoclinic to about  $13 \times 10^{-6}/^\circ\text{C}$  for all cubic phase. The CTE of the filament is not known. A mismatch in CTE between filament and matrix could cause stresses during thermal cycling. The fact that specimens thermally cycled in air did not degrade significantly suggests that an initial mismatch in CTE was not the cause for degradation in those thermally cycled in the corrosive atmosphere. The CTE of various

sodium aluminates, however, could be much different from that of  $\text{Al}_2\text{O}_3$ . Dell and Moseley<sup>7</sup> reported a value of  $\sim 8 \times 10^{-6}/^\circ\text{C}$  for  $\text{Na}_2\text{O} \cdot 11 \text{Al}_2\text{O}_3$ , and values of  $\sim 8 \times 10^{-6}$  and  $7 \times 10^{-6}/^\circ\text{C}$  for the  $a$  and  $c$  axes of  $\text{Na}_2\text{O} \cdot 5 \text{Al}_2\text{O}_3$ , respectively, in the temperature range 25 to  $900^\circ\text{C}$ ; however, Parlier, Sassolas, and Boilot<sup>8</sup> reported values of  $8 \times 10^{-6}$  and  $27 \times 10^{-6}/^\circ\text{C}$  for the  $a$  and  $c$  axes of  $\text{Na}_2\text{O} \cdot 11 \text{Al}_2\text{O}_3$ , respectively, in the temperature range 200 to  $700^\circ\text{C}$ . Substantial anisotropy in CTEs of the sodium aluminates would cause stresses and, probably, microcracking during thermal cycling. Such stresses could have contributed to the observed degradation of specimens heat-treated in the corrosive atmosphere.

In addition, the filament/matrix interface is often designed to allow slip of the filament in the matrix under high stress. The original sintering temperature for the composites in this study was maintained low enough to prevent significant interaction and bonding between filament and matrix; consequently, the matrix material did not sinter to high density. Thus, slip between the filament and matrix might have been possible initially. The amount of porosity in the as-fabricated composites was 20 to 30%, which allowed penetration of  $\text{Na}_2\text{CO}_3$  into the matrices. In the  $\text{Al}_2\text{O}_3$  matrix composite, formation of sodium aluminates in a surface layer minimized attack of the filament below the surface as shown in Figs. 17 and 23; but in the  $\text{ZrO}_2$  matrix composites, the  $\text{Na}_2\text{CO}_3$  migrated through the matrix to react with and form sodium aluminates with the filaments.

Sodium aluminates can be formed from powder mixtures of various ingredients. Youngblood et al.<sup>9</sup> calcined a mixture of  $\text{Al}_2\text{O}_3$ ,  $\text{Na}_2\text{CO}_3$ , and either  $\text{LiNO}_3$  or  $\text{Li}_2\text{C}_2\text{O}_4$  at 800 to  $1000^\circ\text{C}$  for 2 h to obtain partial reaction, then at  $1250^\circ\text{C}$  for 2 h to complete the reaction, while Hind and Roberts<sup>10</sup> heated mixtures of  $\text{Na}_2\text{O} \cdot \text{Al}_2\text{O}_3$  and  $\text{Al}_2\text{O}_3$  in the range 1250 to  $1650^\circ\text{C}$  to form sodium aluminates. The volume expansion of 15% or more of these new compounds, relative to the  $\text{Al}_2\text{O}_3$  from which they formed, is postulated to have

affected the mechanical behavior of the filament/matrix interface. Thermal cycling generated stresses, which caused disruption of the structure by bending, cracking, and spalling.

## SUMMARY AND CONCLUSIONS

Tubular ceramic composite specimens consisting of wound PRD166 continuous filament ( $\text{Al}_2\text{O}_3$ -20 wt %  $\text{ZrO}_2$ ) impregnated with  $\text{Al}_2\text{O}_3$  and  $\text{ZrO}_2$  matrices were heat-treated in air and in an oxidizing atmosphere containing  $\text{Na}_2\text{CO}_3$  vapor. The heat treatments consisted of heating to about  $1150^\circ\text{C}$  in 24 h, holding for 100 or 200 h, then furnace cooling to room temperature. Specimens heat-treated in air had diameter and length changes  $\leq \pm 0.5\%$ , and no other visual evidence of degradation. Specimens heat-treated in the corrosive atmosphere, however, had changes up to about +6%, and those with  $\text{ZrO}_2$  matrices exhibited bending, cracking, and spalling. A specimen with an  $\text{Al}_2\text{O}_3$  matrix and hoop-wound filaments exhibited the least visual evidence of degradation, but also had significant dimensional changes. Optical microscopy revealed a reaction layer at the filament/matrix interface of specimens with a  $\text{ZrO}_2$  matrix. Electron microprobe analysis identified Na in the reaction zone, and X-ray diffraction identified several sodium aluminate compounds. The cumulative evidence indicates that  $\text{Na}_2\text{CO}_3$  migrated through the  $\text{ZrO}_2$  matrix and reacted with the filaments. In the case of the specimen with the  $\text{Al}_2\text{O}_3$  matrix, Na was concentrated in a reaction layer on the surface, and did not react significantly with filaments below the surface layer. X-ray diffraction did not reveal the presence of sodium zirconate in any of the specimens, but did reveal monoclinic, tetragonal, and cubic forms of  $\text{ZrO}_2$ . These forms were definitely present in the filament and, probably, in the matrix.

The following conclusions concerning the use of these materials in atmospheres containing Na-containing compounds can be made:

1. Specimens heat-treated in the corrosive atmosphere had substantially larger dimensional changes than specimens heat-treated in air.
2.  $\text{Na}_2\text{CO}_3$  reacted with  $\text{Al}_2\text{O}_3$  in the filament and matrix to form sodium aluminate compounds.
3. Formation of sodium aluminates, which have a lower density than  $\text{Al}_2\text{O}_3$ , caused a volume expansion.
4. The volume expansion associated with formation of sodium aluminates in the filament of specimens with  $\text{ZrO}_2$  matrices caused the observed degradation, possibly by affecting the mechanical behavior of the filament/matrix interface.
5. The presence of monoclinic and tetragonal forms of  $\text{ZrO}_2$  in the filament and matrix was not particularly detrimental in the air tests, and, therefore, probably not detrimental in the tests in the corrosive atmosphere. However, the volume changes associated with transformation of these phases in an uncontrolled microstructure could act synergistically with new compound formation and might be more important in frequently thermally cycled materials.
6. The results do not indicate a choice between hoop- and helical-wound filaments, because specimens with both types of winding exhibited large dimensional changes and other typical modes of degradation.
7. The results do not indicate a clear choice between the two matrix materials; however, an  $\text{Al}_2\text{O}_3$  matrix protected the filament better than a  $\text{ZrO}_2$  matrix. In addition,  $\text{Al}_2\text{O}_3$  has a lower coefficient of thermal expansion (CTE) than  $\text{ZrO}_2$ , the CTE of  $\text{Al}_2\text{O}_3$  probably better matches the CTE of the filament, and the material has no potentially destructive phase transformations as does partially stabilized  $\text{ZrO}_2$ . For these reasons,  $\text{Al}_2\text{O}_3$  would be preferred for the matrix material.

## ACKNOWLEDGMENTS

The author gratefully acknowledges the assistance of others in the performance of this work: W. P. Parks, Jr., and D. L. Hindman, Babcock & Wilcox Company, who supplied the composite specimens and aided in interpretation of results; P. J. Jones, who conducted the corrosion tests; and J. R. Mayotte, who prepared ceramographic samples and photomicrographs. T. J. Henson, who performed electron microprobe analyses and prepared photomicrographs, and O. B. Cavin, who performed X-ray diffraction analyses, are especially acknowledged for their persistence in gathering and interpreting information. I thank H.-Ee Kim and C. S. Yust for reviewing the draft and for their many helpful suggestions. I also thank A. J. Moorhead and M. A. Karnitz for helpful discussions and interpretation of results. Finally, I thank G. R. Carter of the Metals and Ceramics Division Records Office for final preparation of this report.

## REFERENCES

1. J. E. Snyder and W. P. Parks, Jr., "Research and Development of a Ceramic Fiber Composite Heat Exchanger--Phase I," DOE contract DE-AC-07-84ID12536-1, Babcock & Wilcox Company, Lynchburg, Va., July 1985.
2. W. P. Parks, Jr., "Research and Development of a Ceramic Fiber Composite Heat Exchanger--Phase II," DOE contract DE-AC-07-84ID12536-2, Babcock & Wilcox Company, Lynchburg, Va., April 1990.
3. J. I. Federer, "High-Temperature Corrosion of Heat Exchanger Materials," to be published in *Ceramics Transactions, The American Ceramic Society*, as proceedings of the International Symposium on Corrosion and Corrosive Degradation of Ceramics at the International Ceramic and Technology Congress, November 1-3, 1989, Anaheim, Calif.

4. Powder Diffraction File, Alphabetical Listing Inorganic Phases 1989, compiled by Joint Committee on Powder Diffraction Standards–International Centre for Diffraction Data, 1601 Park Lane, Swarthmore, Pa.
5. E. M. Levin, H. F. McMurdie, and M. K. Reser (ed.), *Phase Diagrams for Ceramists 1975 Supplement*, The American Ceramic Society, Columbus, Ohio, 1975, pp. 88-89.
6. R. Stevens and J. G. P. Binner, "Review-Structure, Properties and Production of Beta-Alumina," *J. Mater. Sci.* **19**, 695-715 (1984).
7. R. M. Dell and P. T. Moseley, "Beta-Alumina Electrolyte for Use in Sodium/Sulfur Batteries, Part 2, Manufacture and Use," *J. Power Sources* **7**, 45-63 (1981/82).
8. M. Parlier, G. Sassolas, and J. P. Boilot, "Dilatometric Study of  $\beta$ -Alumina Single Crystals," *Solid State Ionics* **2**, 185-189 (1981).
9. G. E. Youngblood et al., "Sintering Processed and Heat Treatment Schedules for Conductive, Lithia-Stabilized  $\beta$ -Al<sub>2</sub>O<sub>3</sub>," *Ceram. Bull.* **56**(2), 206-12 (1977).
10. D. Hind and E. W. Roberts, "Densification Kinetics of Na-Beta-Alumina," *Trans. J. Br. Ceram. Soc.* **80**, 219-21 (1981).

## INTERNAL DISTRIBUTION

- |        |                               |        |                               |
|--------|-------------------------------|--------|-------------------------------|
| 1-2.   | Central Research Library      | 30-34. | M. A. Karnitz                 |
| 3.     | Document Reference Section    | 35.    | J. R. Keiser                  |
| 4-5.   | Laboratory Records Department | 36.    | J. O. Kiggans, Jr.            |
| 6.     | Laboratory Records, ORNL RC   | 37.    | E. L. Long, Jr.               |
| 7.     | ORNL Patent Section           | 38.    | D. J. McGuire                 |
| 8-10.  | M&C Records Office            | 39.    | A. J. Moorhead                |
| 11.    | R. L. Beatty                  | 40.    | A. C. Schaffhauser            |
| 12.    | P. F. Becher                  | 41.    | B. W. Sheldon                 |
| 13.    | T. M. Besmann                 | 42.    | G. M. Slaughter               |
| 14.    | A. Bleier                     | 43.    | W. E. Smith                   |
| 15.    | R. S. Carlsmith               | 44.    | D. P. Stinton                 |
| 16.    | P. T. Carlson                 | 45.    | V. J. Tennery                 |
| 17.    | D. R. Childress               | 46.    | T. N. Tiegs                   |
| 18.    | D. F. Craig                   | 47.    | J. R. Weir                    |
| 19.    | J. H. DeVan                   | 48.    | D. F. Wilson                  |
| 20.    | J. R. DiStefano               | 49.    | A. D. Brailsford (Consultant) |
| 21-25. | J. I. Federer                 | 50.    | Y. A. Chang (Consultant)      |
| 26.    | E. L. Fuller, Jr.             | 51.    | H. W. Foglesong (Consultant)  |
| 27.    | C. R. Hubbard                 | 52.    | J. J. Hren (Consultant)       |
| 28.    | D. R. Johnson                 | 53.    | M. L. Savitz (Consultant)     |
| 29.    | R. R. Judkins                 | 54.    | J. B. Wachtman (Consultant)   |

## EXTERNAL DISTRIBUTION

55. AIRESEARCH MANUFACTURING COMPANY, 2525 W. 190th Street,  
Torrance, CA 90509  
D. M. Kotchick
56. BABCOCK AND WILCOX, R&D Division, 1562 Beeson Street, Alliance,  
OH 44601  
C. L. DeBellis
- 57-58. BABCOCK AND WILCOX, P.O. Box 11165, Lynchburg, VA 24505  
E. A. Barringer  
D. L. Hindman

- 59-60. CARBORUNDUM COMPANY, P.O. Box 337, 1625 Buffalo Ave.,  
Niagara Falls, NY 14302  
C. Ebel  
R. Storm
61. CARBORUNDUM COMPANY, P.O. Box 1054, Niagara Falls, NY 14302  
M. C. Kerr
62. CONSOLIDATED NATURAL GAS, 11001 Cedar Avenue, Cleveland, OH 44106  
J. Bjerklie
63. COORS CERAMICS CO., 17750 West 32 Ave., Golden CO 80401  
J. Sibold
64. COORS PORCELAIN COMPANY, 600 Ninth Street, Golden, CO 80501  
R. Kleiner
65. DOW CORNING CORPORATION, 3901 South Saginaw Road, Midland,  
MI 48640  
W. H. Atwell
66. DREXEL UNIVERSITY, Building 27-439, Philadelphia, PA 19104  
F. Ko
- 67-69. GAS RESEARCH INSTITUTE, 8600 W. Bryn Mawr Ave., Chicago, IL 60631  
S. Freedman  
M. A. Lukasiewicz  
C. Stala
70. GENERAL ELECTRIC COMPANY, GE Corporate Research and Development,  
11120 S. Norwalk Blvd., Sante Fe Springs, CA 90670  
J. A. Mears
- 71-72. GENERAL ELECTRIC COMPANY, GE Corporate Research and Development,  
P.O. Box 8, Schenectady, NY 12301  
H. W. Lake, Bldg. KW, Rm. C258  
F. N. Mazandarany, Bldg. K-1, MB-259
73. GENERAL MOTORS CORPORATION, Allison Gas Turbine Division,  
BF Goodrich, Aerospace, P.O. Box 420, Indianapolis, IN 46206-0420  
C. Wilkes

74. IDAHO NATIONAL ENGINEERING LABORATORY, P.O. Box 1625,  
Idaho Falls, ID 83415  
B. W. Brown
75. MASSACHUSETTS INSTITUTE OF TECHNOLOGY, 77 Mass. Ave.,  
Rm. 12-009, Cambridge, MA 02139  
J. S. Haggerty
76. NORTON COMPANY, Worcester, MA 01606  
B. D. Foster
77. PAR ENTERPRISE, INC., 12601 Clifton Hunt Lane, Clifton, VA 22024  
W. J. Rebello
78. PENNSYLVANIA STATE UNIVERSITY, 201 Steidle Building, University Park,  
PA 16801  
R. E. Tressler
79. PENNSYLVANIA STATE UNIVERSITY, 408 Walker Building, University Park,  
PA 16802  
J. R. Hellmann
80. POWER GENERATION CONSULTANTS, 1261 Post House Lane, Media,  
PA 19063  
M. DeCorso
- 81-82. REFRACTORY COMPOSITES, INC., 12220-A Rivera Rd., Whittier,  
CA 90606  
K. Kratsch  
E. L. Paquette
83. SOLAR TURBINES INCORPORATED, P.O. BOX 85376, San Diego,  
CA 92138-5376  
M. Van Roode
84. STONE & WEBSTER ENGINEERING CORPORATION, 245 Summer Street,  
Boston, MA 02107  
R. A. Rosenberg
85. SULLIVAN MINING CORPORATION, P.O.Box 4615, San Diego, CA 92121  
T. M. Sullivan

86. TECHNICAL CERAMICS LABS, 568 Prospect Ave., Grand Island, NY 14072  
P. T. B. Shaffer
87. TEXTRON, INC., 2 Industrial Ave., Lowell, MA 01851  
B. N. Thompson
88. UNIVERSITY OF ILLINOIS AT CHICAGO, P.O. Box 4348, Chicago, IL 60680  
M. J. McNallan
89. UNIVERSITY OF TENNESSEE SPACE INSTITUTE, MS 3, Tullahoma,  
TN 37388  
W. H. Boss
- 90-91. U.S. DOE, CHICAGO OPERATIONS OFFICE, 9800 S. Cass Avenue, Argonne,  
IL 60439  
J. E. Jonkouski  
J. Mavec
92. U.S. DOE, DIVISION OF WASTE ENERGY REDUCTION, 1000 Independence  
Ave., S.W., Washington, DC 20585  
J. N. Eustis
93. U.S. DOE, IDAHO OPERATIONS OFFICE, 550 Second Street, Idaho Falls,  
ID 83401  
G. R. Peterson
- 94-96. U.S. DOE, OFFICE OF INDUSTRIAL TECHNOLOGIES, 1000 Independence  
Avenue, Forrestal Building, Washington, DC 20585  
J. Eustis  
W. P. Parks, Jr.  
S. L. Richlen
- 97-98. U.S. DOE, OAK RIDGE OPERATIONS OFFICE, P.O. Box 2001,  
Oak Ridge, TN 37831-8600  
M. J. Rohr  
Assistant Manager for Energy Research and Development
- 99-108. U.S. DOE, OFFICE OF SCIENTIFIC AND TECHNICAL INFORMATION,  
P.O. Box 62, Oak Ridge, TN 37831

For distribution by microfiche as shown in DOE/OSTI-4500,  
Distribution Category UC-310 [Industrial Programs (General)]